

2017

# Finite Element Analysis of Boat Suspension

Desheng Yao  
*Lehigh University*

Follow this and additional works at: <https://preserve.lehigh.edu/etd>



Part of the [Mechanical Engineering Commons](#)

---

## Recommended Citation

Yao, Desheng, "Finite Element Analysis of Boat Suspension" (2017). *Theses and Dissertations*. 2931.  
<https://preserve.lehigh.edu/etd/2931>

This Thesis is brought to you for free and open access by Lehigh Preserve. It has been accepted for inclusion in Theses and Dissertations by an authorized administrator of Lehigh Preserve. For more information, please contact [preserve@lehigh.edu](mailto:preserve@lehigh.edu).

# **Finite Element Analysis of Boat Suspension**

**by**

**Desheng Yao**

**A Thesis**

**Presented to the Graduate and Research Committee**

**of Lehigh University**

**in Candidacy for the Degree of**

**Master of Science**

**in**

**Mechanical Engineering**

**Lehigh University**

**August 2017**



© Copyright by Desheng Yao 2017  
All Rights Reserved

---

## Certificate of approval

This thesis is accepted and approved in partial fulfillment of the requirements for the Master of Science.

---

Date

---

Thesis Advisor

---

Co-Advisor

---

Chairperson of Department

---

## Acknowledgement

I would first like to thank my thesis advisor Professor J.L. Grenestedt of the Composites Lab. The door to Prof. Grenestedt office was always open whenever I ran into trouble or had a question about my research or writing. He consistently allowed this paper to be my own work, but steered me in the right direction whenever he thought I needed it. I would also like to thank other students in the Composite Lab: Jake, Zhangning, Chao, Longfu and Lean. They helped me enthusiastically whenever I was in trouble during this project.

Finally, I must express my very profound gratitude to my parents and to my family for providing me with unfailing support and continuous encouragement throughout my years of study and through the process of researching and writing this thesis. This accomplishment would not have been possible without them. Thank you.

---

# TABLE OF CONTENTS

List of Figures	Page Vi
List of Tables	Page Viii
Abstract	1
Introduction	2
Finite Element Method Introduction	2
Suspension Boat Introduction	3
Design and Analysis of Bungs for Attaching Suspension to Hull	5
Analyses of the Front Suspension Links	18
Contact Mechanics Introduction	21
Contact in Abaqus and Sample for Contact	21
Analysis of Two Suspension Link	28
Simpler Model for Analysis	34
Analysis of Stick Model	35
Linear Analysis of Suspension Links	44
Results Analysis of Linear Elastic Simulation	49
Conclusion	51
References	52
Vita	52

---

## LIST OF FIGURES

Fig.1 Example of suspension boat	3
Fig.2 Sketch of suspension boat being built	4
Fig.3 Sketch of where bungs will be used to install suspension components to the center hull	6
Fig.4 Initial design of the bung	6
Fig.5 Diagram of $\alpha$ and assembly for simulation	7
Fig.6 Holes on base plate and on flange of the bung	8
Fig.7 Boundary conditions to connect the bung and the base plate	8
Fig.8 Boundary condition and load for analysis	10
Fig.9 Von Mises stresses for $\alpha = 15^\circ$	11
Fig.10 Von Mises stresses for $\alpha = 45^\circ$	11
Fig.11 Von Mises stresses for wall thickness 3-5mm	13
Fig.12 Von Mises stresses for wall thickness 3-4mm	13
Fig.13 Von Mises stresses for wall thickness 3-4.5mm	14
Fig.14 Stresses on the fillet for $\alpha = 15^\circ$ (fillet radius 24mm)	15
Fig.15 Stresses on the fillet for $\alpha = 45^\circ$ (fillet radius 24mm)	15
Fig.16 Stresses on the fillet for $\alpha = 15^\circ$ (fillet radius 20mm)	16
Fig.17 Stresses on the fillet for $\alpha = 15^\circ$ (fillet radius 16mm)	16
Fig.18 Manufactured bung	17
Fig.19 Two suspension arms for the left front sponson	18
Fig.20 Sample result of SolidWorks	19
Fig.21 Asymmetry of stress distribution	20
Fig.22 Contact definition in Abaqus	22
Fig.23 Hard contact Pressure-Clearance relationship	23
Fig.24 Exponential Pressure-Clearance relationship	24
Fig.25 Contact parameter sample	25
Fig.26 Stress analysis for hard contact	26

---

Fig.27 Stress analysis (Pressure 300MPa, Clearance 0.11mm)	26
Fig.28 Stress analysis (Pressure 800MPa, Clearance 0.01mm)	27
Fig.29 Meshed model	28
Fig.30 Finer mesh of joints	28
Fig.31 Suspension link on the boat	29
Fig.32 Boundary conditions at upper boundary arm	31
Fig.33 Boundary condition and load at lower boundary arm	31
Fig.34 Angle between upper arm and lower arm	32
Fig.35 Simplified model	33
Fig.36 Diagram of coupling constrain	33
Fig.37 Tentative stress analysis result	34
Fig.38 Stick model	36
Fig.39 Element numbers for the upper and lower suspension links	37
Fig.40 Node numbers	37
Fig.41 the latest FE model	45
Fig.42 Analysis results under load case 400ax	46
Fig.43 Stresses by joint A for 400ax	46
Fig.44 Stresses by joint B for 400bx	47
Fig.45 Analysis Results of Joint A and B for case 400abx	47
Fig.46 Stresses by joint A for 400abx	48
Fig.47 Stresses by joint A for 400abx	48
Fig.48 Stress concentrations by joint A	49
Fig.49 Stresses in joint A	50

---

## LIST OF TABLES

Table-1 Properties of A316L Stainless Steel	9
Table-2 Max Stress and Corresponding $\alpha$	10
Table-3 Calibrating Parameters	25
Table-4 Forces on elements for -100a load case	40
Table-5 Forces on elements for -100b load case	40
Table-6 Forces on elements for 0a load case	41
Table-7 Forces on elements for 0b load case	41
Table-8 Forces on elements for 200a load case	42
Table-9 Forces on elements for 200a load case	42
Table-10 Forces on elements for 400a load case	43
Table-11 Forces on elements for 400a load case	43

---

## ABSTRACT

A suspension boat concept was developed and patented by Grenestedt [1.1] to reduce high vertical accelerations which plague small boats operating at high speed. The suspension boat under consideration consists of a center hull and four sponsons connected to suspension links, springs and shock absorbers. The suspension links will be heavily loaded during operation of the boat. A two-seat manned suspension boat is presently being built and the purpose of this thesis was to analyze suspension components for this boat.

First, a stainless-steel bung used for attaching suspension components to the center hull was analyzed, and modified to increase strength and reduce mass. Stress analyses were performed under different loading conditions. Different wall thicknesses and fillet radii were studied. A good configuration was developed and manufactured.

Second, two suspension links connecting a front sponson to the center hull were analyzed. Initially contact mechanics were used in finite element analyses of the links, but this was not very successful. Various simplifications were then made in order to be able to analyze the links using linear analysis. The results are believed to be of sufficient accuracy for design of the hardware for the boat.

---

## Introduction

### Finite Element Method Introduction

Modern technological advances give engineers great challenge on increasing complex projects. To get a better understanding, analysts need mathematical models to simulate behavior of complex system. Engineering sciences are utilized to describe the behavior of physical systems in the form of partial differential equations. The finite element method (FEM) is a numerical approach by which partial differential equations can be solved approximately. From an engineering standpoint, FEM is a method for solving engineering problems by computer simulation.

The finite element method consists of using a simple approximation of unknown variables to transform partial differential equations into algebraic equations. It draws on the following three disciplines:

- I. Engineering sciences to describe physical laws (partial differential equations);
- II. Numerical methods for the elaboration and solution of algebraic equations;
- III. Computing tools to carry out the necessary calculations efficiently using a computer.

Nowadays, the finite element method has become one of the most frequently used methods in simulation and computation. This method could solve a large number of problems in practice, including many steady and transient problems in linear and nonlinear regions for one-, two- and three-dimensional domains.

---

## Suspension Boat Introduction

Small boats operating at high speeds often suffer from very high vertical accelerations.

This acceleration will impose large loads on the boats as well as on the occupants. A boat concept with suspension was developed to reduce vertical accelerations [1.1, 1.2]. It consists of a center hull that is generally not in contact with the water and one or more sponsons connected to suspension links, springs and shock absorbers. Fig.1 shows an example of a small-scale suspension boat [1.2]. In Fig.1, there is a main hull and four suspended sponsons.

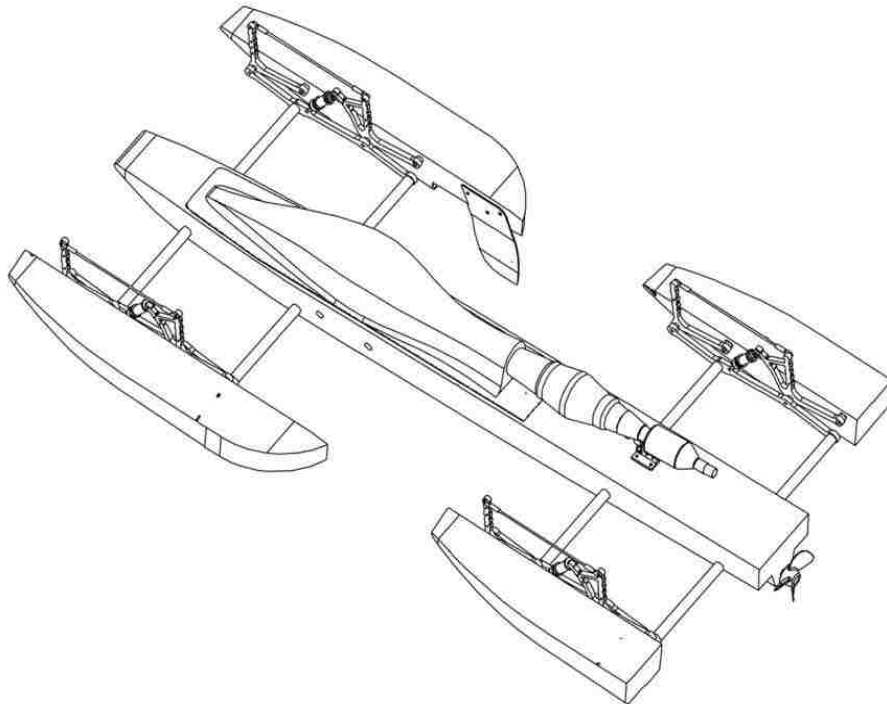


Fig.1 Example of Suspension Boat

---

Numerical simulations were performed by Grenestedt [1.1], and the results indicate that the analyzed suspension boat could operate at 60 knots in sea state three without seeing vertical accelerations above 1.5G. The same boat but with rigidly mounted running surfaces would see an order of magnitude higher vertical accelerations.

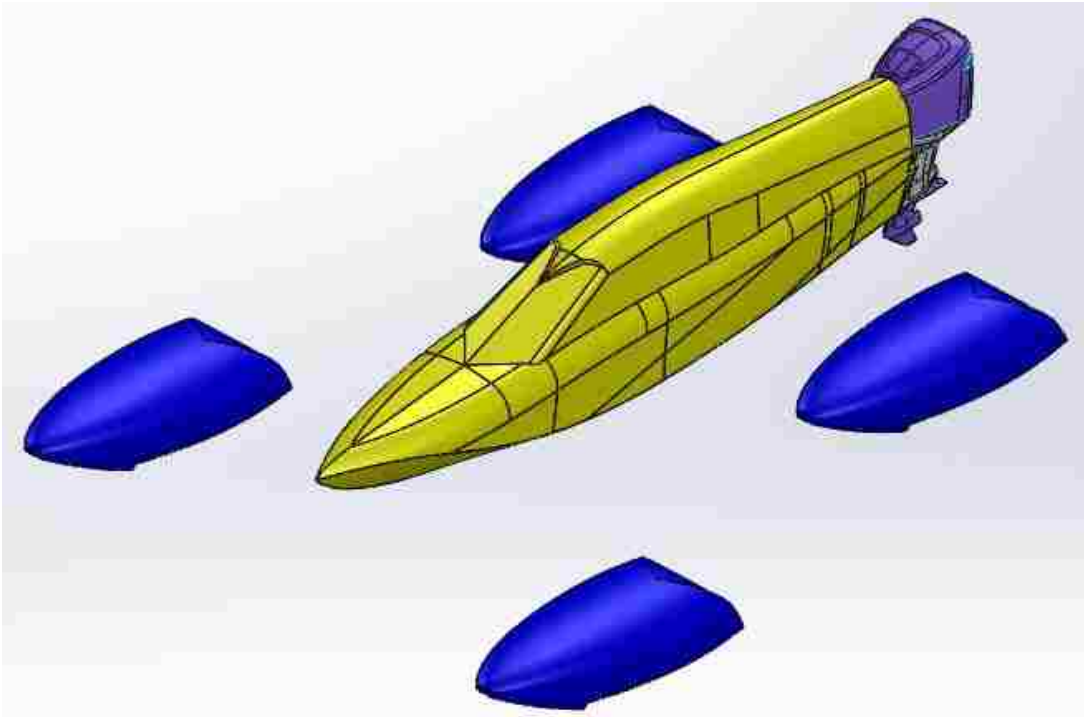


Fig.2 Sketch of suspension boat presently being built (suspension components are hidden)

---

## Design and Analysis of Bungs for Attaching Suspension to Hull

SolidWorks is a solid modeling CAD and CAE software. It also provides simulation package to optimize and validate a design effectively. SolidWorks simulation uses the displacement formulation of the finite element method to calculate displacements, strains, and stresses under internal and external loads. For displacement formulation, node displacements are the only unknown. Solution of the equilibrium equations leads to node displacement, which are used to calculate element stress.

A stainless-steel bung was designed and tested in SolidWorks. This bung will be used to attach suspension components to the center hull. In the present design, there are eighteen such bungs on the boat. The bung will be welded to the end of stainless steel tubes which make up supports to which suspension arms and shock absorbers will be attached. As Figure 3 shows, this bung will be installed on the center hull at different locations (some of the bung are not displayed). Due to layout of the suspension components and the center hull, tubes will be welded to the bung at different angles. The angle between bungs and tubes  $\alpha$  varies between  $15^\circ$  and  $45^\circ$  at different locations of the boat. A number of numerical analyses were performed for bungs with tubes connected at different angles. In particular,  $\alpha$  in Fig.5 was varied between  $15^\circ$  and  $45^\circ$ . The initial design of the bung is shown in Fig.4. The bung consists of three portions: vertical wall (cylindrical outside and conical inside), flange and fillet. The inner diameter of the vertical wall increase from the bottom to the top.

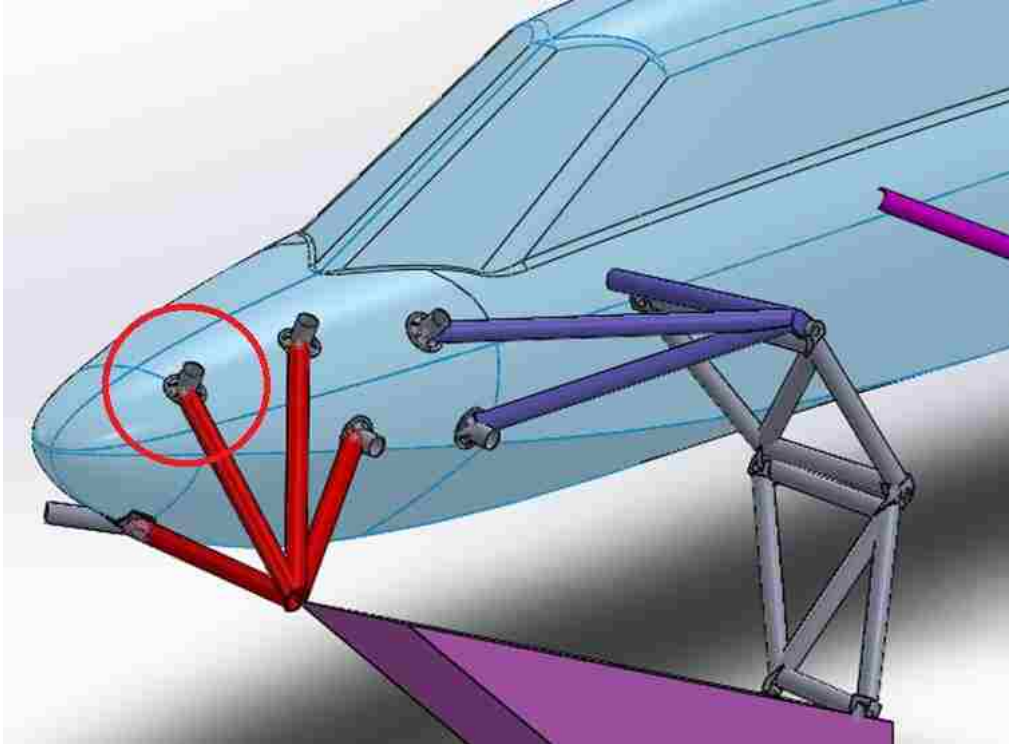


Fig.3 Sketch of where bungs will be used to install suspension components to the center hull. One of the bungs is circled.

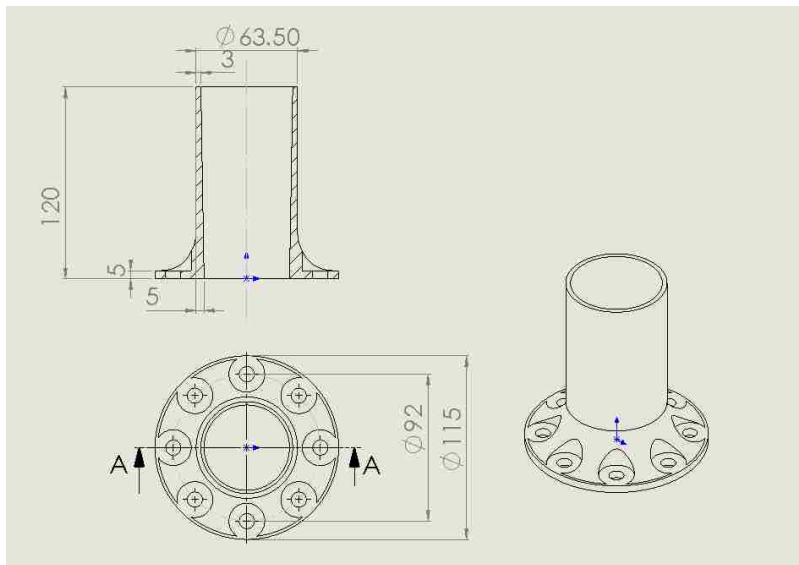


Fig.4 Initial design of the bung; all dimensions in [mm]

---

The bungs are connected to the hull by bolts. A simplified model used to analyze the bung is shown in Fig.5. It consists of the stainless-steel bung, a 7075 Aluminum base plate (10mm thick and 300mm diameter) which was simply supported along its edges (roughly representing the center hull), and a short piece of stainless steel tubing (300mm long, 63.5mm outer diameter and 1.65mm wall thickness) which was connected to the bung and loaded in tension at its free end. There were eight holes on the base plate and on the flange of the bung representing bolt holes as shown in Fig.6. A simplified approach to model the bolted connection was used: the lower edge of the holes in the bung were connected to the upper edge of the holes in the base plate. The two connected edges are shown in Fig.7. Different models with angles of  $\alpha$  from  $15^\circ$  to  $45^\circ$  were analyzed. The material of the bung and the tubing is A316L stainless steel, mechanical properties of which are listed in Table 1.

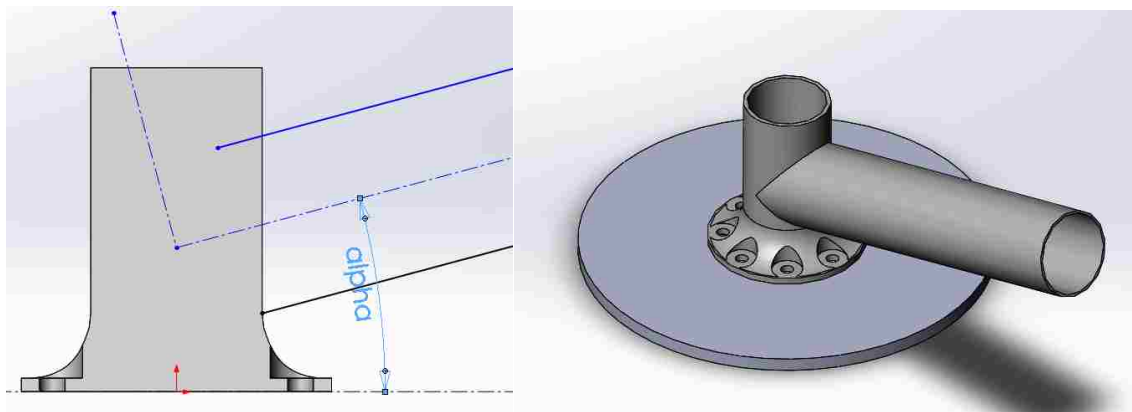


Fig.5 Diagram of  $\alpha$  and assembly for simulation

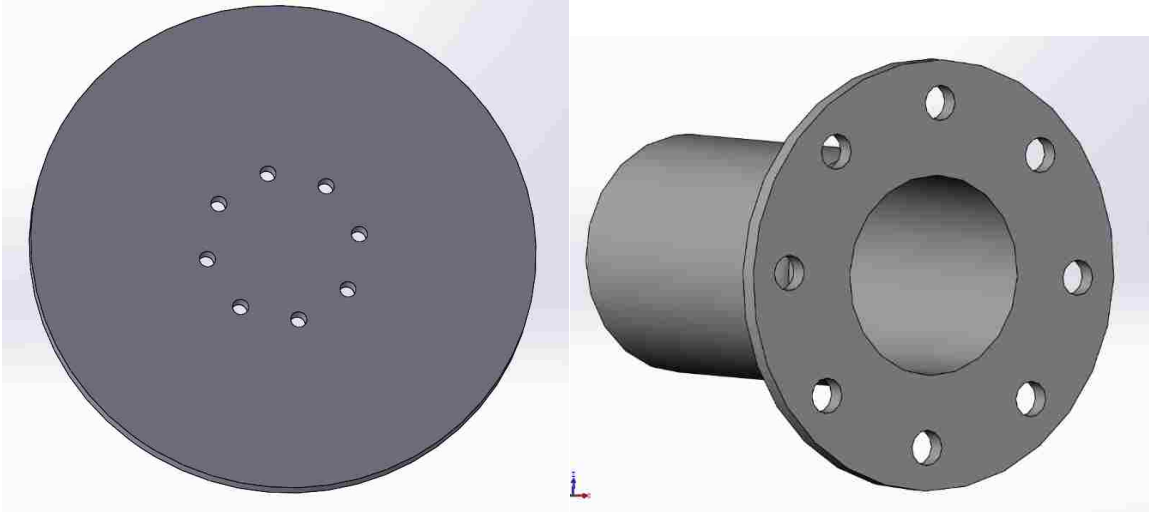


Fig.6 Holes on base plate (left) and on flange of the bung (right)

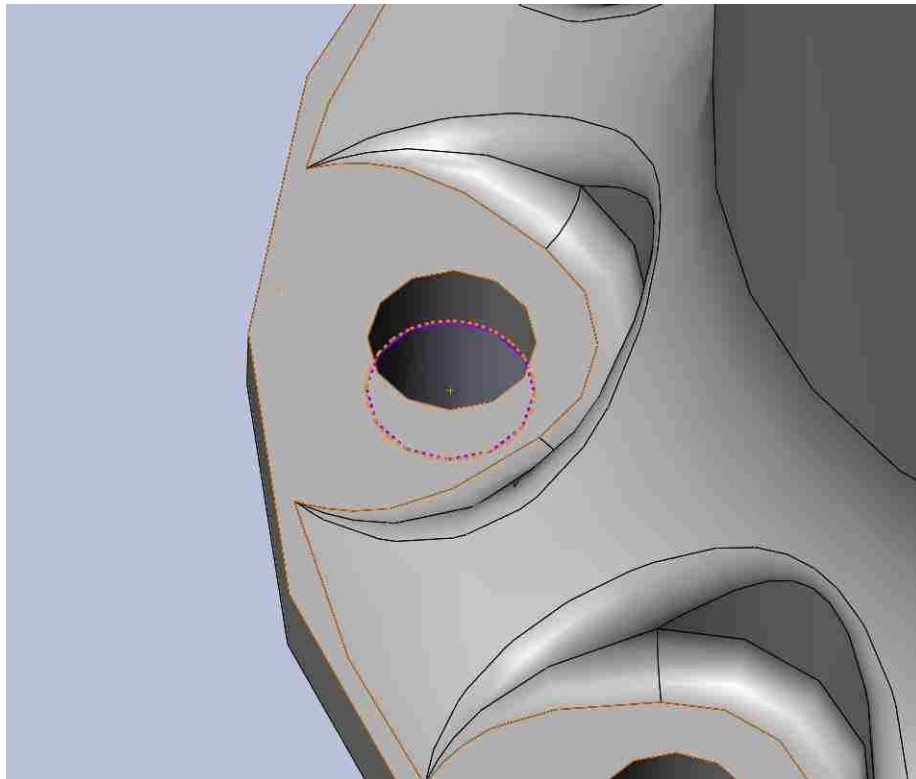


Fig.7 Boundary conditions to connect the bung and the base plate

Table-1 Properties of A316L stainless steel

Property	Density	Yield Strength	Ultimate Strength	Elongation at Break	Modulus of Elasticity
Value	8000kg/m <sup>3</sup>	290MPa	560MPa	50%	193GPa

The goal of the analyses and modifications of the design was to find a lightweight design with sufficient strength. Low mass is desired to reduce loads, improve handling, increase speed, reduce fuel consumptions, etc. The von Mises stresses inside the vertical wall were analyzed first because suspension components will be welded to the vertical wall of this bung. The stress distribution of the fillet portion was analyzed later.

Finite element models were made for  $\alpha$  of 15°, 20°, 25°, 30°, 35°, 40° and 45°. A  $10^5\text{N}$  load was applied to the far-end surface of the attached tube as shown in Fig.8. This load was considerably higher than it is believed to occur during normal operation. However, in extreme cases, such load may be approached. The design does not need to consider fatigue at this high load level. Rather, local plastic yielding would be acceptable if loads at this level were ever encountered. Purely linear elastic analyses were therefore performed, disregarding the fact that the material would yield at 290 MPa and considerably higher stresses were obtained in fairly small regions.

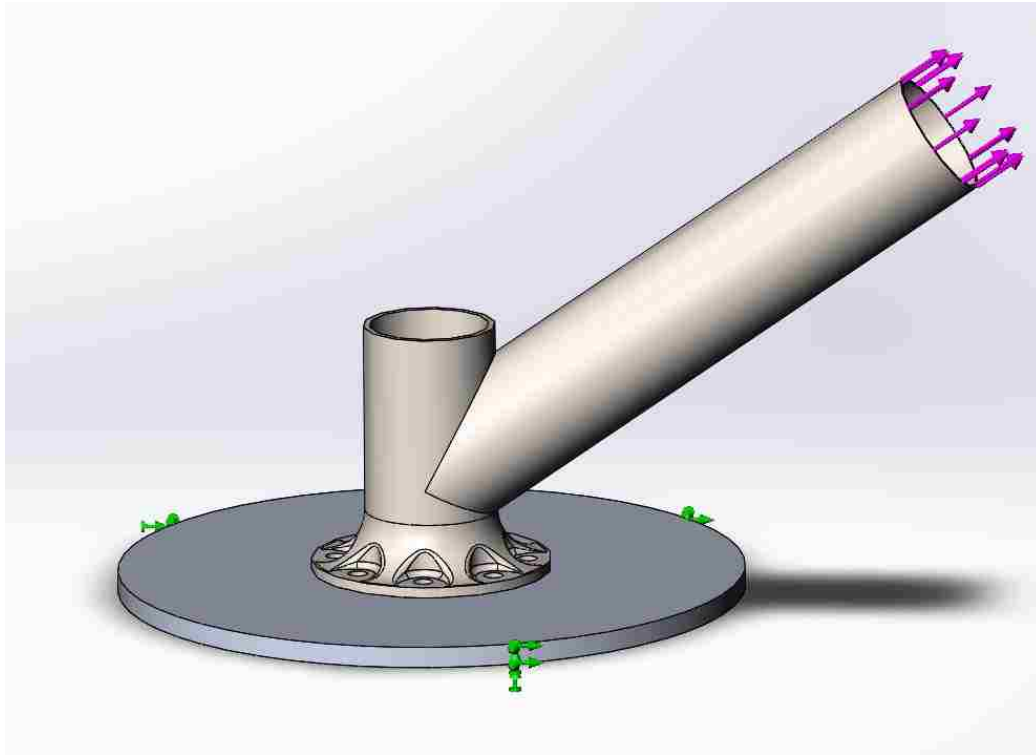


Fig.8 Boundary condition and load for analysis

Maximum stress inside vertical wall corresponding to different  $\alpha$  is listed in Table 2.

These maximum stresses showed up at the place like red portion inside the vertical wall as Fig.9 shows.

The highest von Mises stresses are found inside the vertical wall for  $\alpha = 15^\circ$  and  $45^\circ$  as shown in Fig.9 and Fig.10.

Table-2 Max stress and corresponding  $\alpha$

$\alpha$ [°]	15	20	25	30	35	40	45
Max Stress[MPa]	493.2	477.3	471.1	453.5	417.1	399	370.1

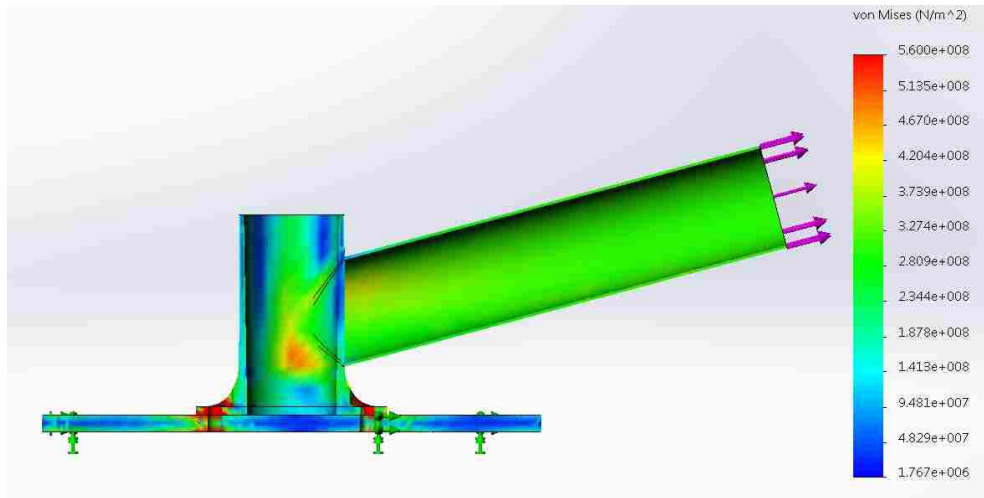


Fig.9 Von Mises stresses for  $\alpha = 15^\circ$

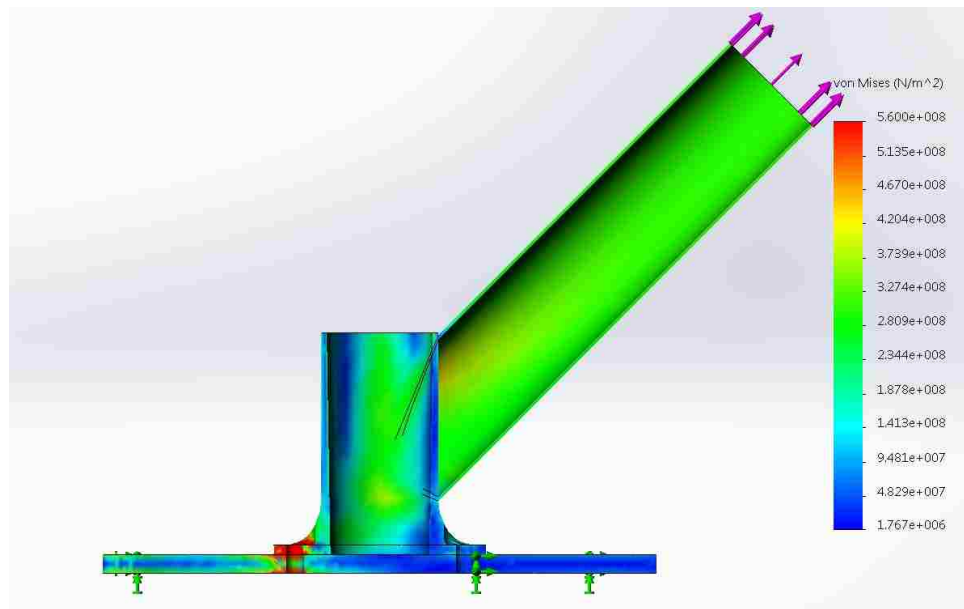


Fig.10 Von Mises stresses for  $\alpha = 45^\circ$

From Table 2 and Fig.9, Fig.10, we can conclude that maximum von Mises stress inside the vertical wall decrease with angle  $\alpha$  increasing. When  $\alpha = 45^\circ$ , the area of highest

---

stresses is quite small. Since the load is applied in  $45^\circ$  direction, the lateral component of applied load decrease to minimum value comparing to smaller  $\alpha$  conditions, for applied load remained 100,000N. Hence the vertical wall would be acted upon by stretching along vertical direction mostly and bending along horizontal direction minorly comparing to smaller  $\alpha$  conditions. And this leads to decrease of stress concentration area. Considering mass of the bung, the wall thickness of vertical wall for large  $\alpha$  could be reduced within allowable stress limit. The wall thickness for initial design was 3 mm at the top and 5 mm at the bottom. Take  $\alpha = 35^\circ$  for example, the max von Mises stress was 417.1MPa inside the vertical wall. To achieve a lighter part, a thinner wall thickness should be considered for load conditions with large  $\alpha$  such as a wall thickness to 3 mm at the top and 4 mm at the bottom. Comparison of von Mises stresses between two models with these different wall thickness is given in Fig.11 and Fig.12. For the latter case, the maximum von Mises stress was 515.5MPa, which may be acceptable. A third analysis was performed with the thickness 3 mm at the top and 4.5 mm at the bottom.

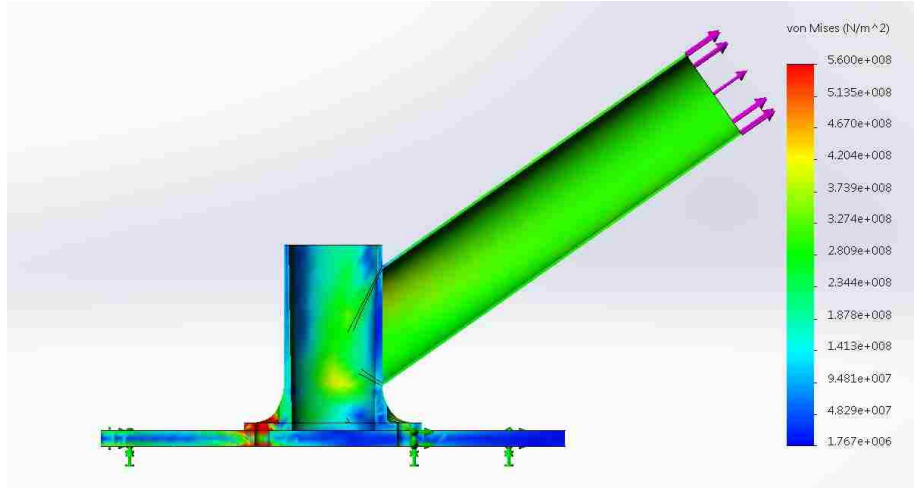


Fig.11 Von Mises stresses for wall thickness 3-5mm

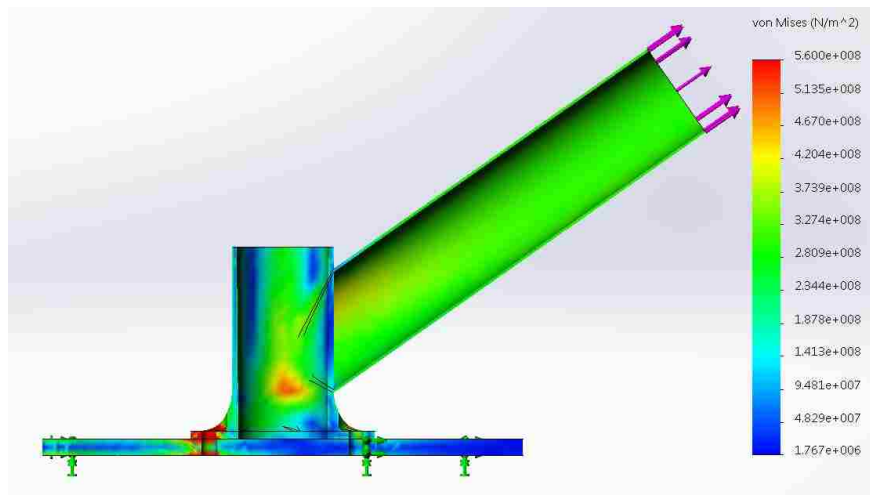


Fig.12 Von Mises stresses for wall thickness 3-4mm

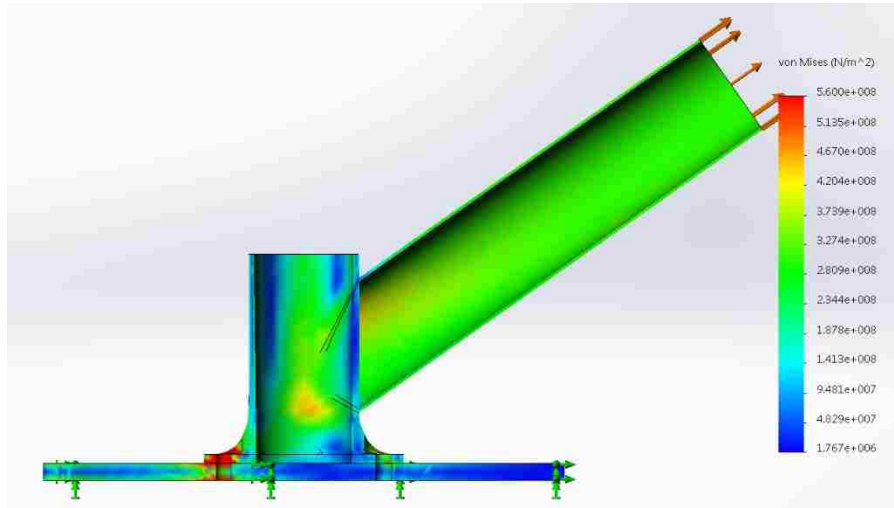


Fig.13 Von Mises stresses for Wall Thickness 3-4.5mm

Fig.13 shows Von Mises stress distribution of simulation with wall thickness 3 mm at the top and 4.5 mm at the bottom. Maximum stress drops to 464.9MPa. This wall thickness is acceptable for this angle  $\alpha = 35^\circ$ . Meanwhile, the mass of the bung decreased 8% with this wall thickness condition (3 and 4.5 mm versus 3 and 5 mm), dropping from 1193g to 1098g.

Next, the effect of different radius of the fillet was studied. The initial fillet radius was 24mm. Stresses on the fillet portion for  $\alpha = 15^\circ$  and  $\alpha = 45^\circ$  are shown in Fig.14 and Fig.15. When  $\alpha$  is large, max stresses were found on the flange opposite to the side below the tube, and for a small  $\alpha$  max stresses were founded on both sides of the flange. For  $\alpha = 15^\circ$ , various fillet radii (20mm, 16mm) were analyzed and results were compared to initial radius result as shown in Fig.16 and Fig.17. As fillet radius decreases, a larger portion of the fillet was under high stress.

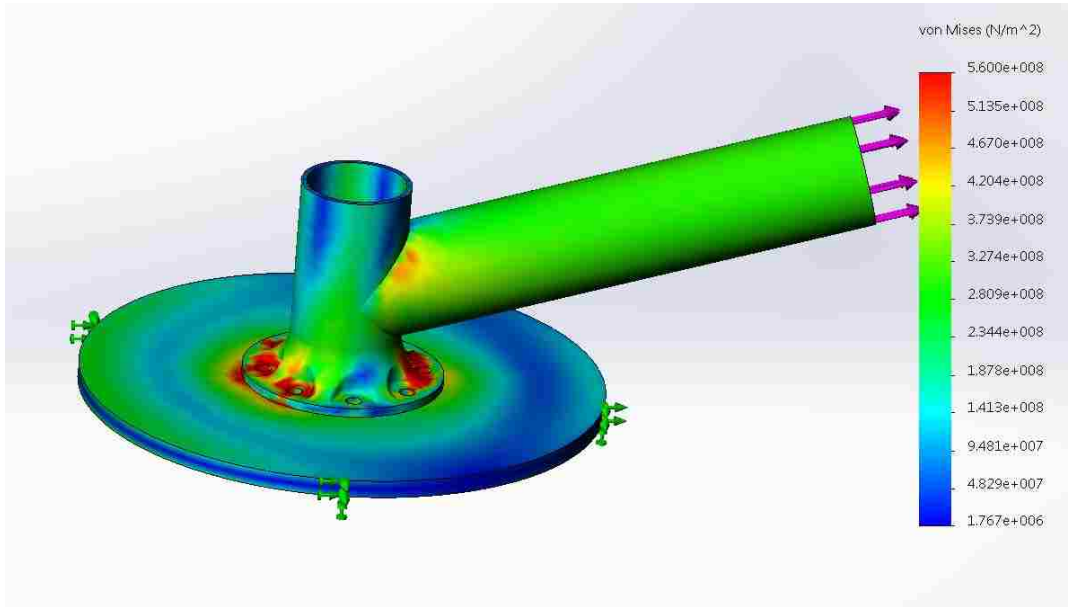


Fig.14 Stresses on the fillet for  $\alpha = 15^\circ$  (fillet radius 24mm)

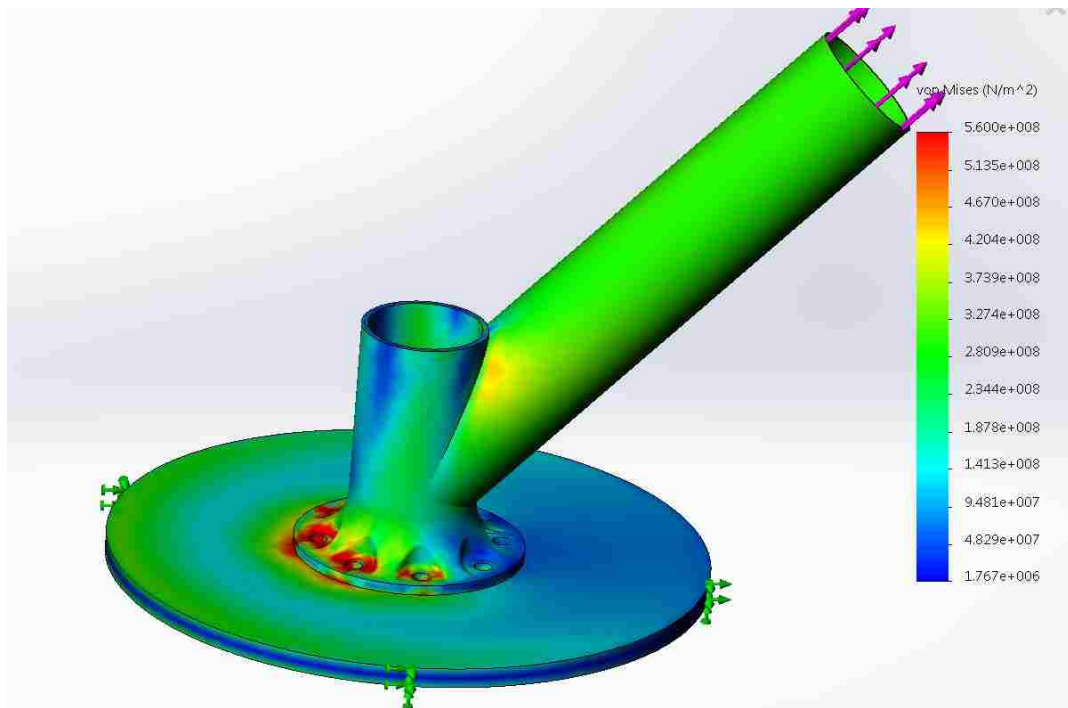


Fig.15 Stresses on the fillet for  $\alpha = 45^\circ$  (fillet radius 24mm)

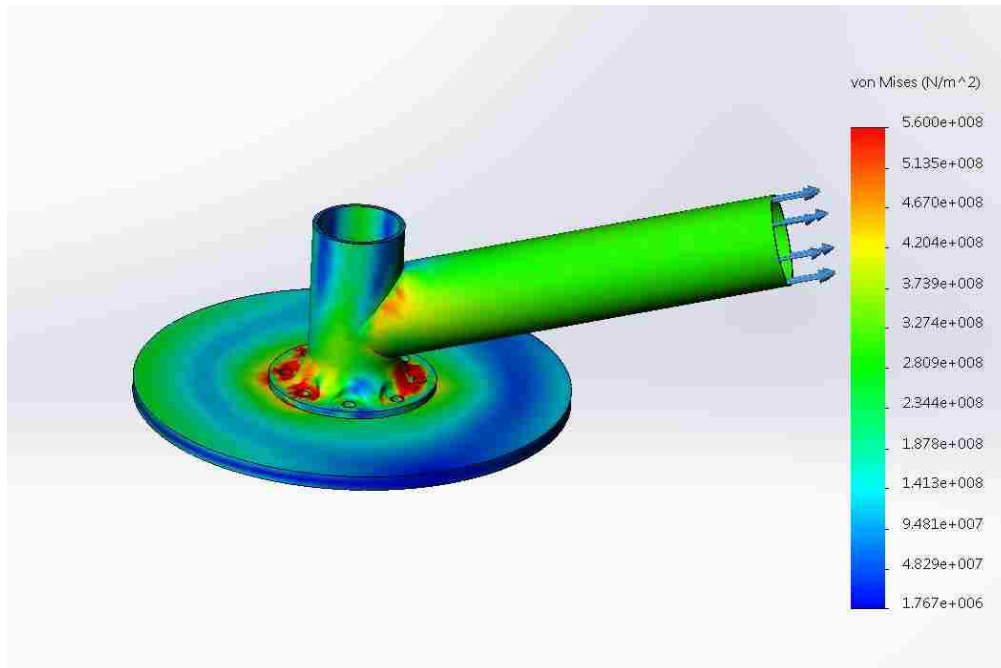


Fig.16 Stresses on the fillet for  $\alpha = 15^\circ$  (fillet radius 20mm)

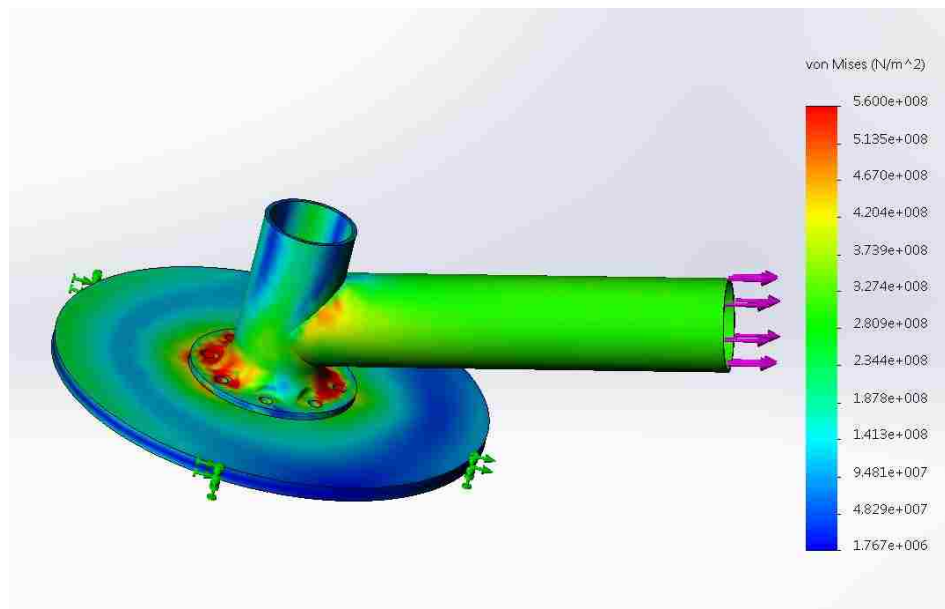


Fig.17 Stresses on the fillet for  $\alpha = 15^\circ$  (fillet radius 16mm)

---

It is found that the bigger fillet radius leads to lower maximum stress on the fillet.

However, the mass of the bung was barely affected by fillet radius. Hence the fillet radius was chosen as 24mm.

Finally, two designs for different situations were determined. For  $\alpha$  ranging from  $15^\circ$  to  $35^\circ$ , initial design parameters are acceptable, for  $\alpha$  larger than  $35^\circ$ , wall thickness of vertical tube 3 mm at the top and 4.5 mm at the bottom is used. In summary, wall thickness of vertical tube 3mm at the top and 4.5mm at the bottom is acceptable for all  $\alpha$  cases. Hence this wall thickness was selected to unify design of the bung, which will improve manufacturing efficiency at the same time.

All the bungs have been manufactured as shown in Fig.18.



Fig.18 Manufactured bung

---

## Analyses of the Front Suspension Links

Fig.19 shows two suspension links for the left front sponsons. They are shown installed on the center hull in Fig.3. There is an upper arm and a lower arm. Each arm contains nine tubes and four joints. Several auxiliary parts like pins and bearings are used to connect the upper and lower arms.

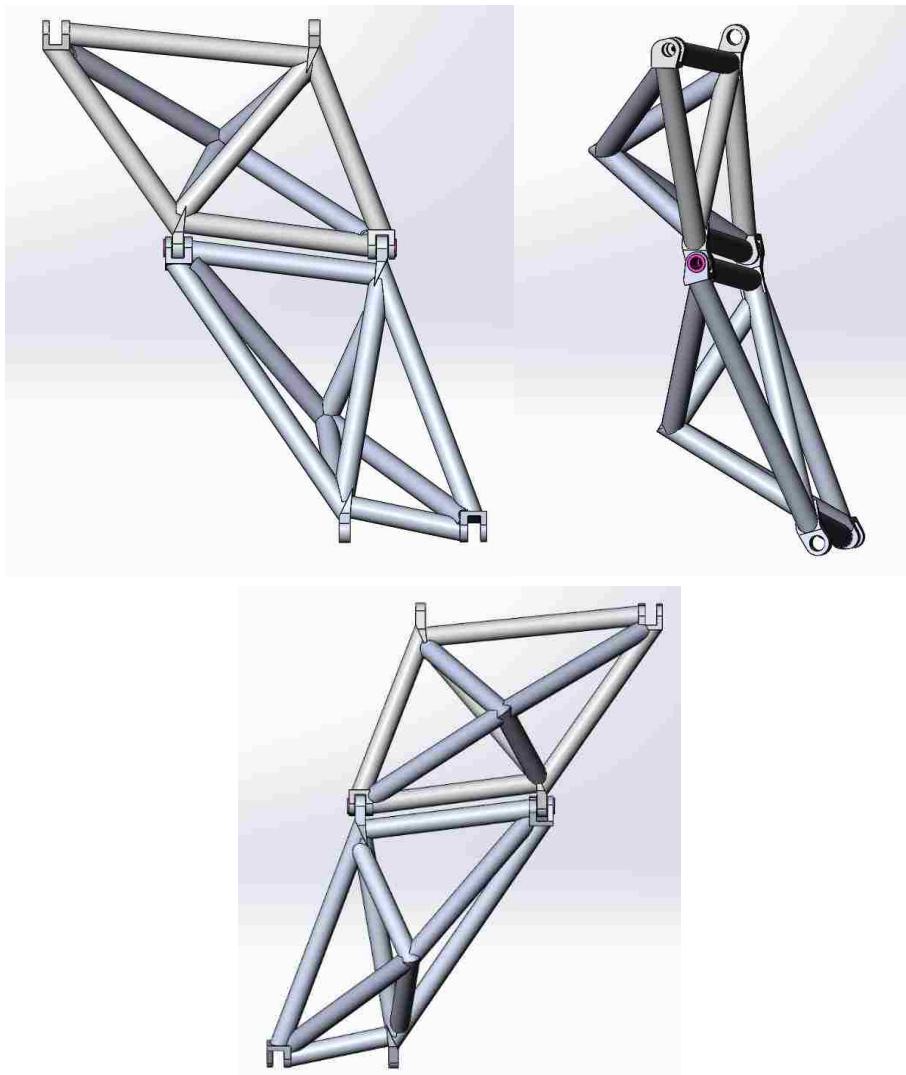


Fig.19 Two suspension arms for the left front sponson (top left: front view; top right: left view; bottom: rear view)

---

Simulation of the suspension is crucial since failure of suspension components could lead to major damage of the boat and the occupants. The finite element analysis of this assembly is more complex than that of the bung in the previous section because contact is involved in the analysis. Contact problems are highly nonlinear and require more computations than a linear elastic analysis. To gain some confidence in the simulations, some simple geometries were first analyzed.

A sample assembly was built in SolidWorks and finite element analyzed. Fig.20 shows the simulation result.

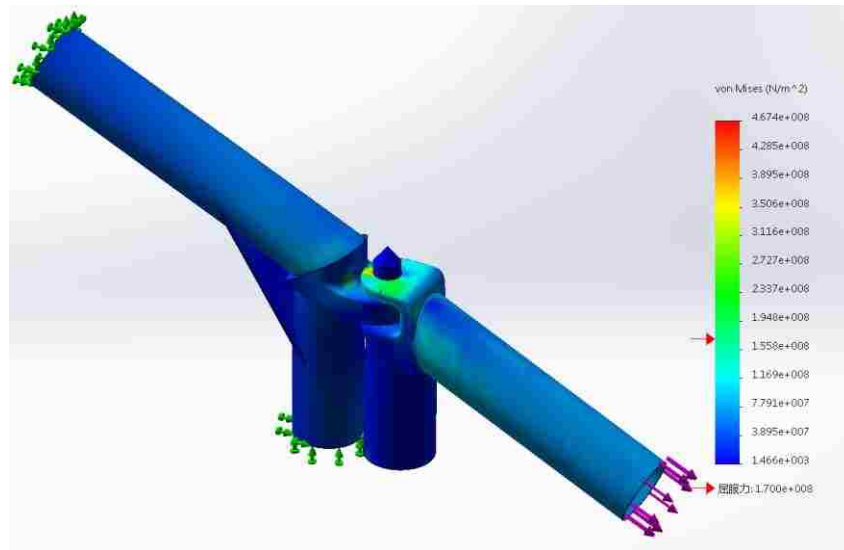


Fig.20 Sample result of SolidWorks

This structure has a symmetry plane, and the boundary conditions and load were applied symmetrically to this plane. Hence, the stress analysis result should be symmetric.

However, asymmetry of stress distribution shows up near the contact area as shown in

---

Fig.21 shows. There are only three types of contact property available in SolidWorks simulation package: non-penetrable, attached and allow-penetrable. Other advanced contact properties could not be modified by user.

Based on this simple calculation, it was concluded that accuracy of the contact algorithm in the SolidWorks simulation package is not acceptable for the present suspension analysis. A more sophisticated FEA (finite element analysis) software is required.

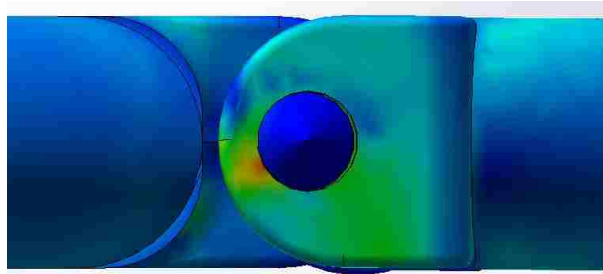


Fig.21 Asymmetry of stress distribution

Abaqus is a powerful FEA package of Dassault Systèmes. It integrates pre-processing, processing and post-processing functions. Abaqus/CAE and Abaqus/Standard were chosen to be used for the present analyses. Abaqus/CAE is a software suite used for both the modeling, analysis of mechanical components and assemblies (pre-processing) and visualization of finite element analysis result. Abaqus/Standard is a general-purpose finite-element analyzer that employs implicit integration.

---

## Contact Mechanics Introduction

In general, contact occurs when bodies touch each other at least at one point in space. 3D objects may have contact with each on shared point(s), line(s) and/or surface(s). Contact mechanics, developed based on the continuum mechanics and mechanics of materials, is a theory to describe pressure and adhesion (normal) and friction (tangential) stresses that arise during shared point/line/surface contact between deformable bodies.

Depending on the geometry and material properties of each deformable body, contact can be high non-linear. Computational modeling of contact is a very challenging topic, and much research work is still being performed in this field. Proper modeling of contact problems requires significant knowledge and experience from the modeler.

## Contact in Abaqus and Sample for Contact

In Abaqus/Standard, contact is defined by:

- I. General Contact: with a single interaction definition, contact is enforced over many or all regions of a model
- II. Contact Pairs: only contact between two surfaces can be described

These are schematically depicted in Fig.22. Each approach in the modeling of contact has its own advantages and limitations. General contact is a more versatile method to deal with contact since contact between disconnected regions of the bodies can be described with a single interaction. Contact pair requires more precise definition of contacting surfaces and has many restrictions on the types of surfaces involved.

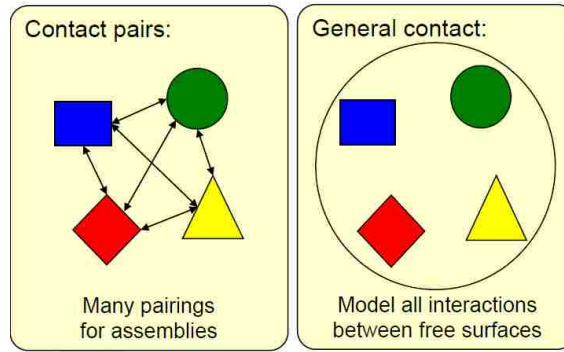


Fig.22 Contact definition in Abaqus

Besides contact type definition, contact problem in Abaqus requires:

- I. definition of bodies that may potentially be in contact.
- II. definition of surfaces that interact during contact.
- III. definition of the properties of surfaces in contact with each other.
- IV. additional contact properties including mechanical properties, thermal properties, etc.
- V. an algorithm to control contact interaction during the simulation.

The surface definition is critical for contact problem. A slave surface and a master surface must be defined in each contact pair, or they would be assigned automatically in general contact. Major difference between master surface and slave surface is that master surface is considered “harder” than slave surface in the program. Abaqus allows nodes on master surface to penetrate slave surface if necessary. On the contrary, nodes on slave surface never penetrate master surface. At the same time, slave surface should be more finely meshed to prevent penetrating master surface from happening.

---

As for algorithm to control contact interaction, default algorithm for normal behavior is “hard contact”. In “hard contact” there is no force between bodies until they touch, and when they touch the force can rise very sharply. This behavior can easily lead to divergence in numerical simulations. Convergence can be improved using an approximate contact behavior in which contact forces build up more slowly as two bodies approach each other. Abaqus provides several algorithms to approximate real contact normal behavior: exponential, linear, tabular and scale factor.

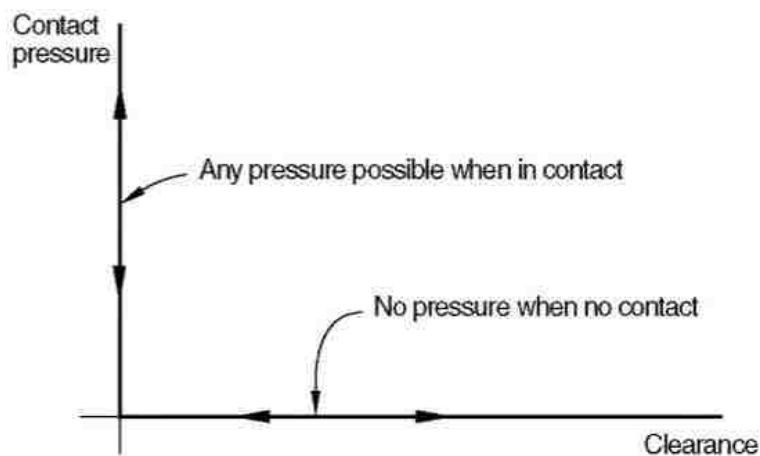


Fig.23 Hard contact Pressure-Clearance relationship

For the suspension assembly presently under investigation, the exponential method was used. Exponential relationship among pressure and clearance is shown in Fig.24.

Selecting the pressure  $p^0$  and the clearance  $c$  properly is crucial for a good approximation of real contact behavior. Meanwhile, divergence maybe be prevented because there is a buffer area to let contact stiffness gradually change.

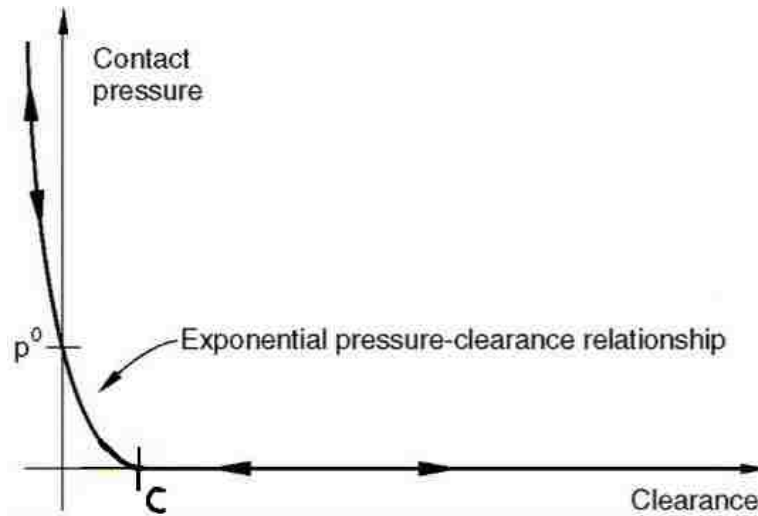


Fig.24 Exponential Pressure-Clearance relationship

However, exponential method will cause some penetration, and analysis step would become unstable if penetration error is too large. To get optimum value for  $p^0$  and  $c$  see above, a sample assembly was first studied. Finite element analyses were performed on the sample assembly shown in Fig.25, using different  $p^0$  and  $c$ . Excepting for some fillets, bearings and pin used in this assembly are identical to those used in the suspension assembly. Besides, contact clearance of this sample is the same as the suspension assembly. Once a set of parameters was determined, they could be directly applied to the suspension assembly.

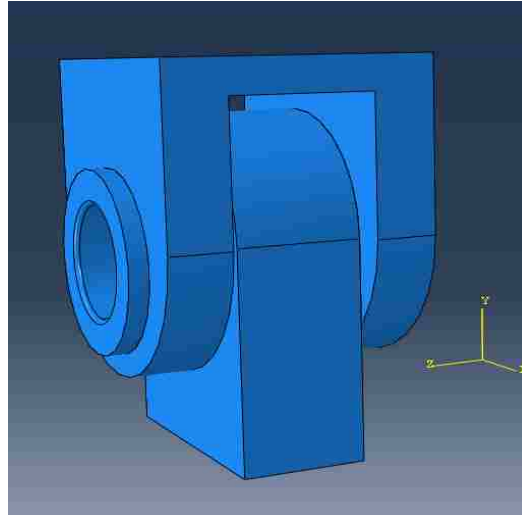


Fig.25 Contact parameter sample

During analysis process, several sets of parameters were used. They are listed in Table 3.

Comparing stress analysis result with analysis result using “hard contact” yields the optimized exponential calibrating parameters. Approximation may be closer to real contact status if the parameter  $p^0$  is larger and parameter  $c$  is smaller, but convergence will be more difficult. Hence, these sets of calibrating parameters were selected. Fig.26-28 show selected simulation results.

Table-3 Calibrating parameters  $p^0$  and  $c$  in the exponential relation

Pressure( $p^0$ )[MPa]	300	400	500	600	700	800
Clearance( $c$ )[mm]	0.11	0.09	0.07	0.05	0.03	0.01

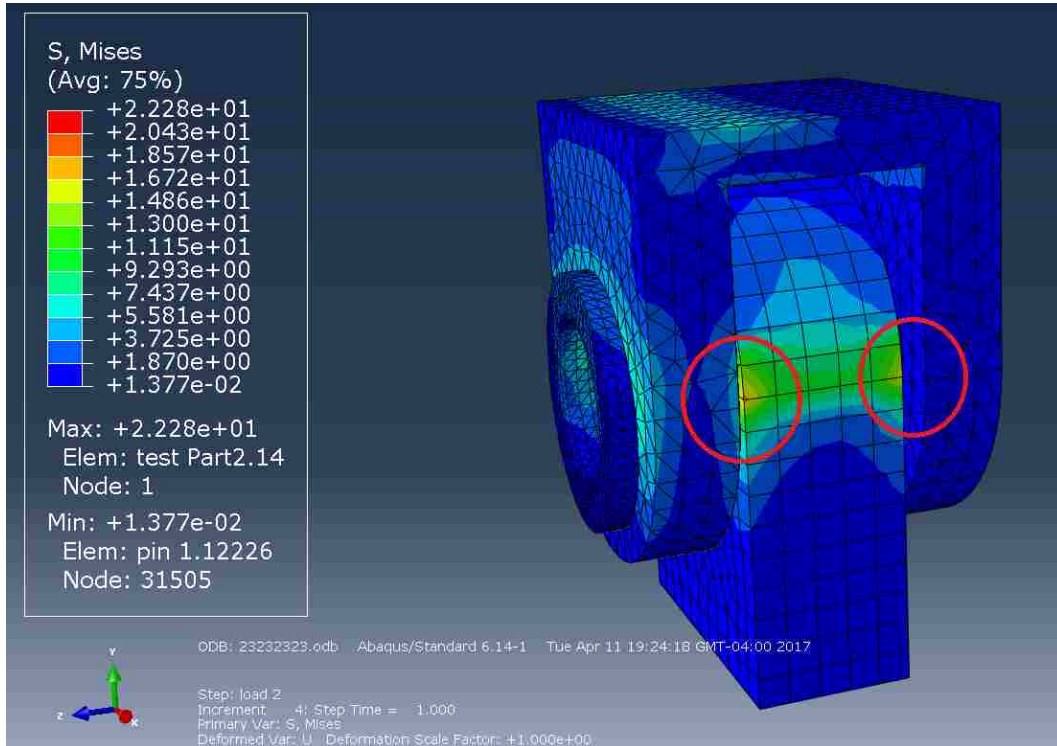


Fig.26 Stress analysis for hard contact

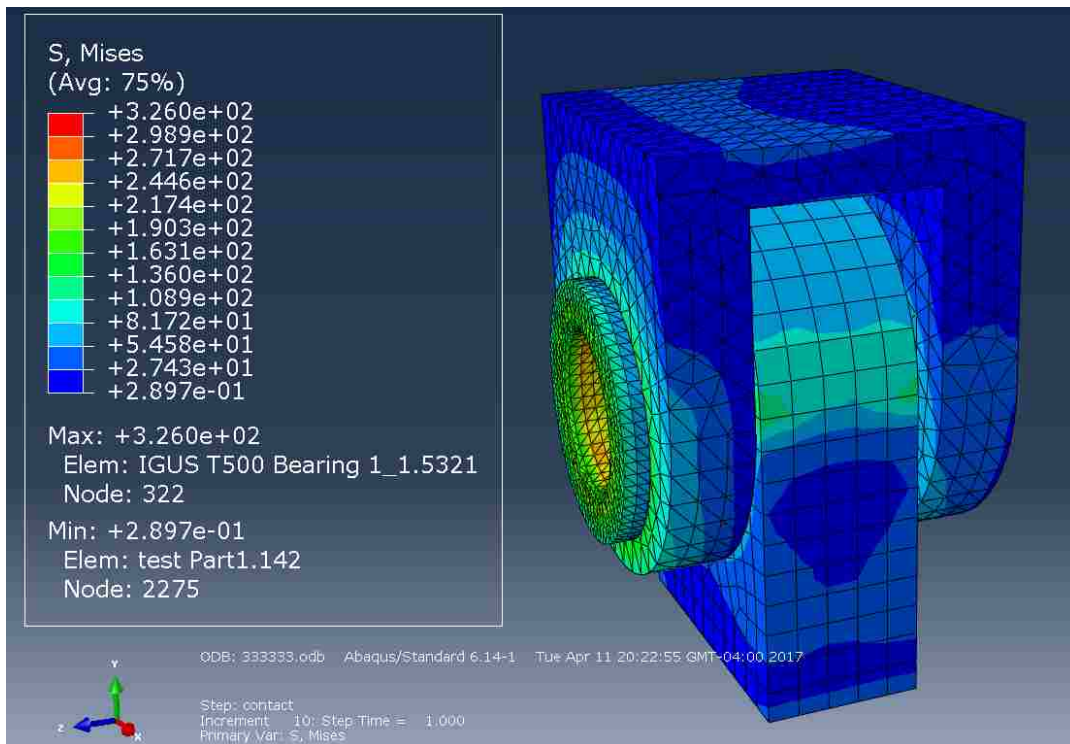


Fig.27 Stress analysis (pressure 300MPa, clearance 0.11mm)

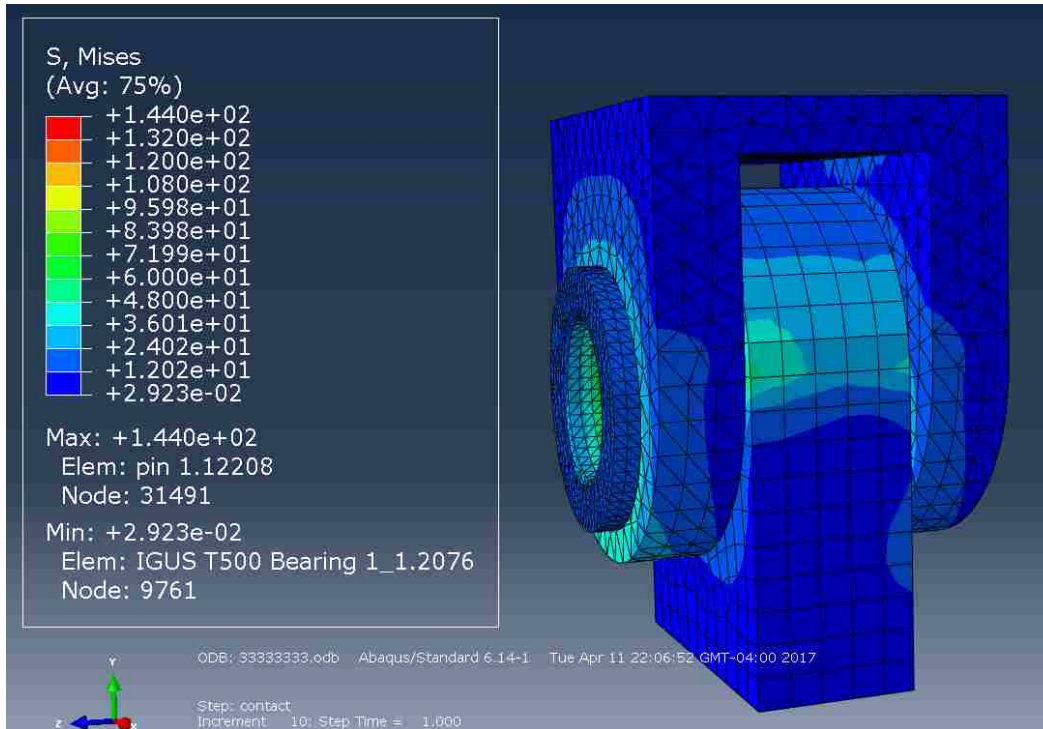


Fig.28 Stress analysis (pressure 800MPa, clearance 0.01mm)

Fig.26 gives that max stress (circled portion) on joint is about 22MPa for “hard contact”. From Fig.27 and Fig.28, max stress at corresponding location on joint is 137MPa and 30MPa for different calibration parameters. Same tendency happens for max stress at pin. Considering exponential Pressure-Clearance relationship as Fig.24, it is clear that exponential approximation would be closer to real contact situation with larger  $p^0$  and smaller  $c$ . In conclusion, the calibrating parameters: pressure  $p^0$  800MPa and clearance  $c$  0.01mm were more accurate approximation parameters and they were selected for subsequent simulations.

---

## Analysis of two suspension links

The suspension links discussed earlier were assembled in SolidWorks then imported to Abaqus/CAE for pre-processing. The FE mesh is shown in Fig.29. To simplify the meshing, each arm was meshed separately and then connected using constraint equations. This is in general not advisable, but due to greater simplicity it was presently used. Fig.30 shows a close up of the joints.

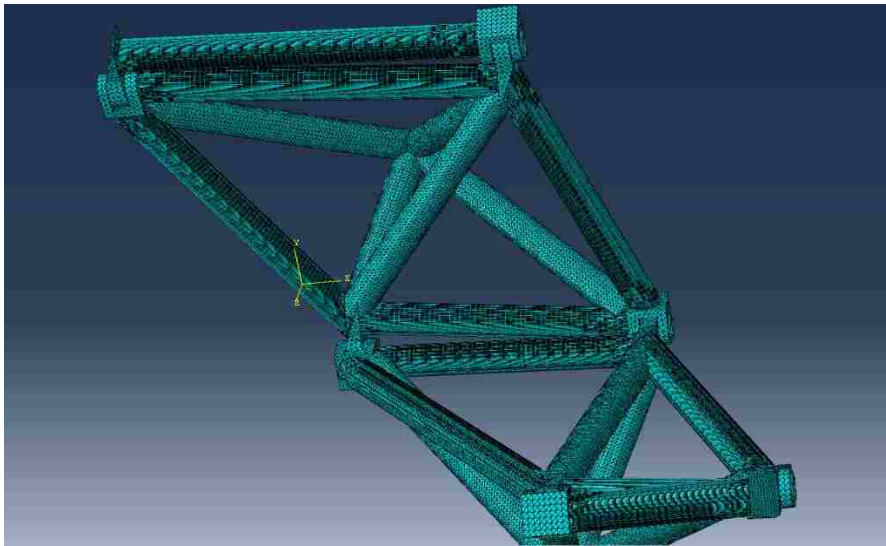


Fig.29 Meshed model

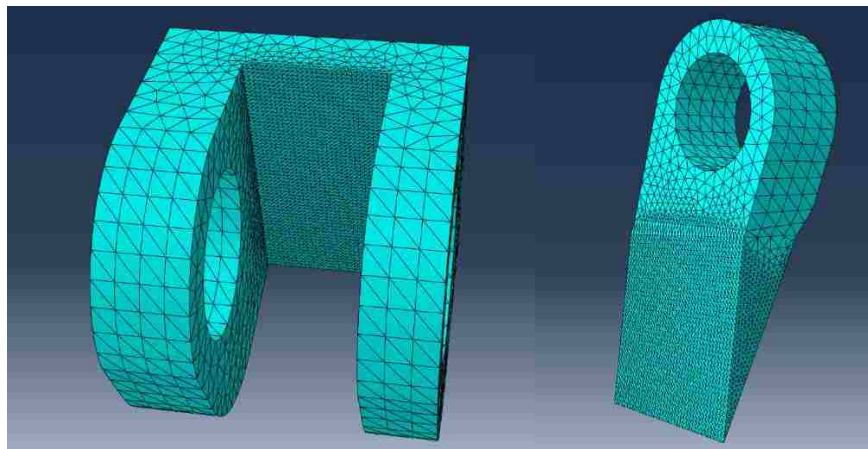


Fig.30 Finer mesh of joints (fillets were added for later analyses)

---

As mentioned, the goal at present was to analyze the two suspension arms. However, in order to introduced the loads in a reasonable fashion two more parts were modeled: an upper support tube which would be connected to the center hull, and a lower hinge assembly that would be attached to a sponson; see circled part in Fig.31.

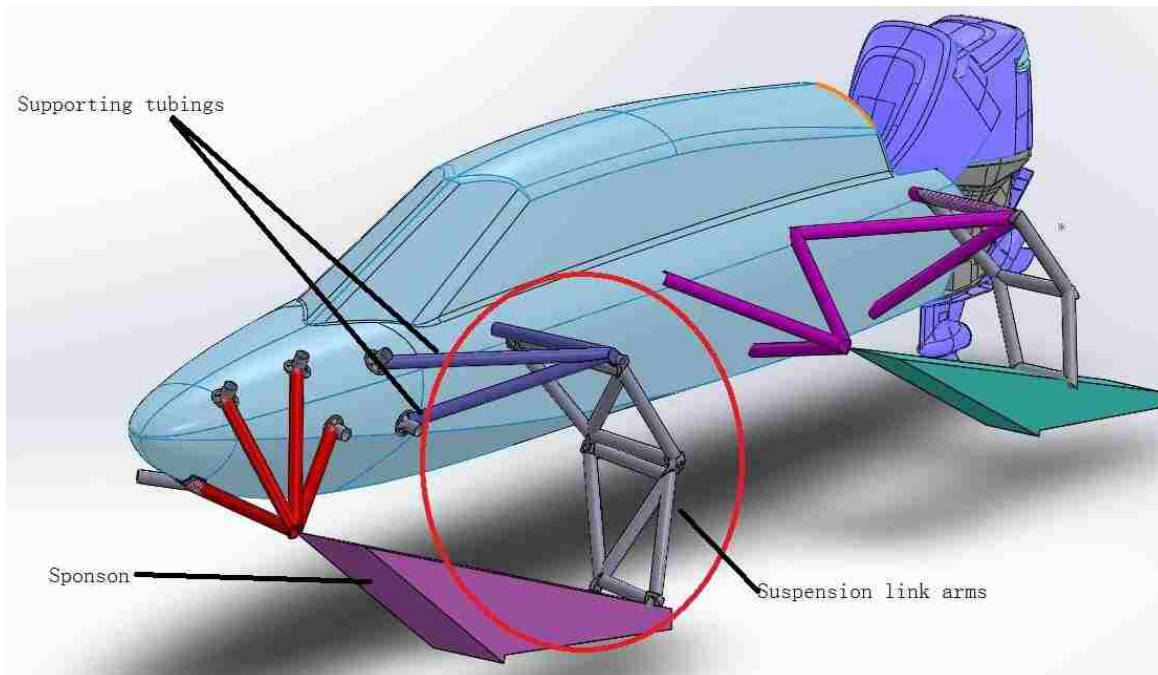


Fig.31 Suspension link on the boat (the sponsons are just place holders and do not represent the real ones)

In this Figure, the upper arm is connected to the center hull and the lower arm is connected to the sponson. A spring and shock absorber will be connected between the center hull and the sponson. The suspension links will be subjected to many different load cases when the water acts on the sponsons. The most severe load case is believed to be horizontal

---

transverse force near the transom of a sponson (vertical loads would lead to the spring and shock absorber compressing and relieving the force). A load of 100,000N in the horizontal direction was chosen to represent the horizontal transverse force. Four different suspension deflections were analyzed: -100mm, 0mm, 200mm and 400mm, where 0mm corresponds to the normal ride height [1.1]. Here, 400mm corresponds to a 400mm deflection upwards of the transom of the front sponson, etc.

Boundary conditions were determined from constraints that constrain suspension link. In the FE model of suspension links as shown in Fig.34, two boundary arms (upper boundary arm and lower boundary arm) were added. These two boundary arms represented tubes that connect the two suspension links to the center hull and to the sponson, and boundary conditions were applied on them to simulate reality. For the upper boundary arm, one end is welded to the bung installed on the center hull and the other end is constrained by two supporting tubes as Fig.31 shows. For the lower boundary arm, under at a given sponson deflection, movements in Y and Z directions of the inboard side are constrained by the sponson and the shock absorber, while the outboard is free. So, the boundary conditions of the FE model as shown in Fig.32 could be represented as:

the inboard side of upper boundary arm:  $U_x = U_y = U_z = 0$ ;

the outboard side of upper boundary arm:  $U_y = U_z = 0$ ;

the inboard side of lower boundary arm:  $U_y = U_z = 0$ .

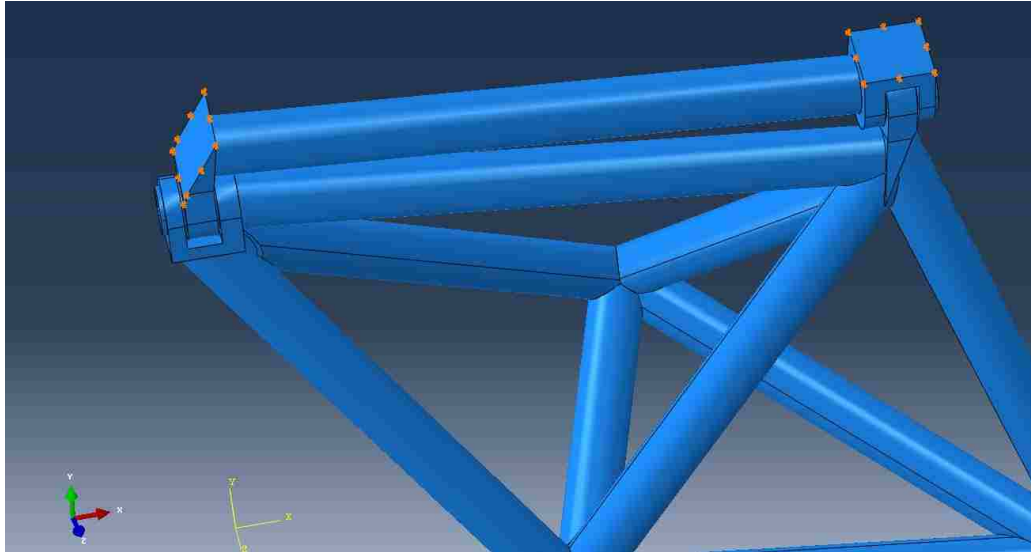


Fig.32 Boundary conditions at upper boundary arm

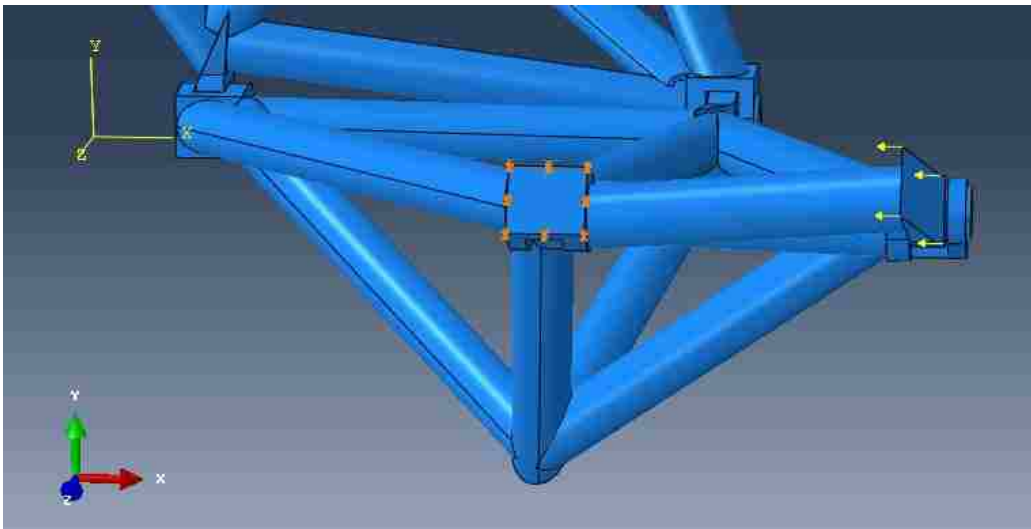


Fig.33 Boundary condition and load at lower boundary arm (the yellow arrows indicate the applied force)

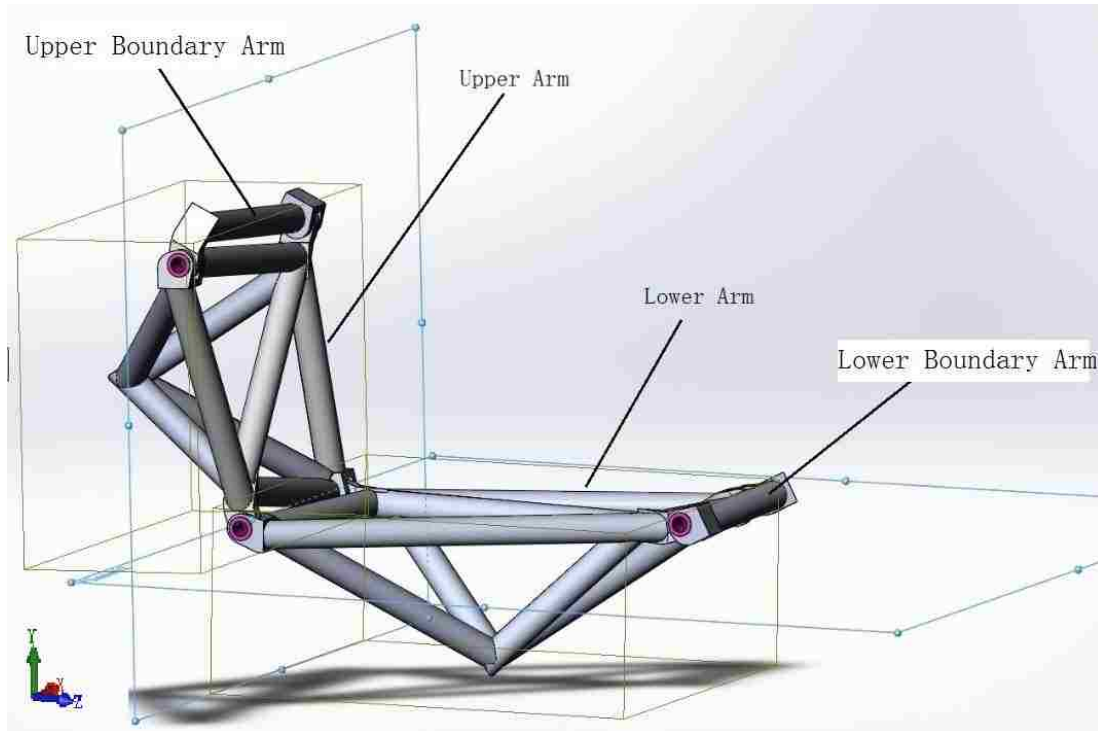


Fig.34 Angle between upper arm and lower arm

Simulation failed due to insufficient hard drive space. There were 761,765 elements in this model, and more than half of these element was for the tubes. To reduce the number of elements in the model, a new FE model was made where beam elements were used rather than 3D solid elements to model the nine tubes of each suspension arm. The simplified model is shown in Fig.35. Boundary conditions and load were the same as in previous analyses. The beams were coupled to the 3D ends of the tubes, such that the initially flat cross section would remain flat and perpendicular to the beam (Fig.36).

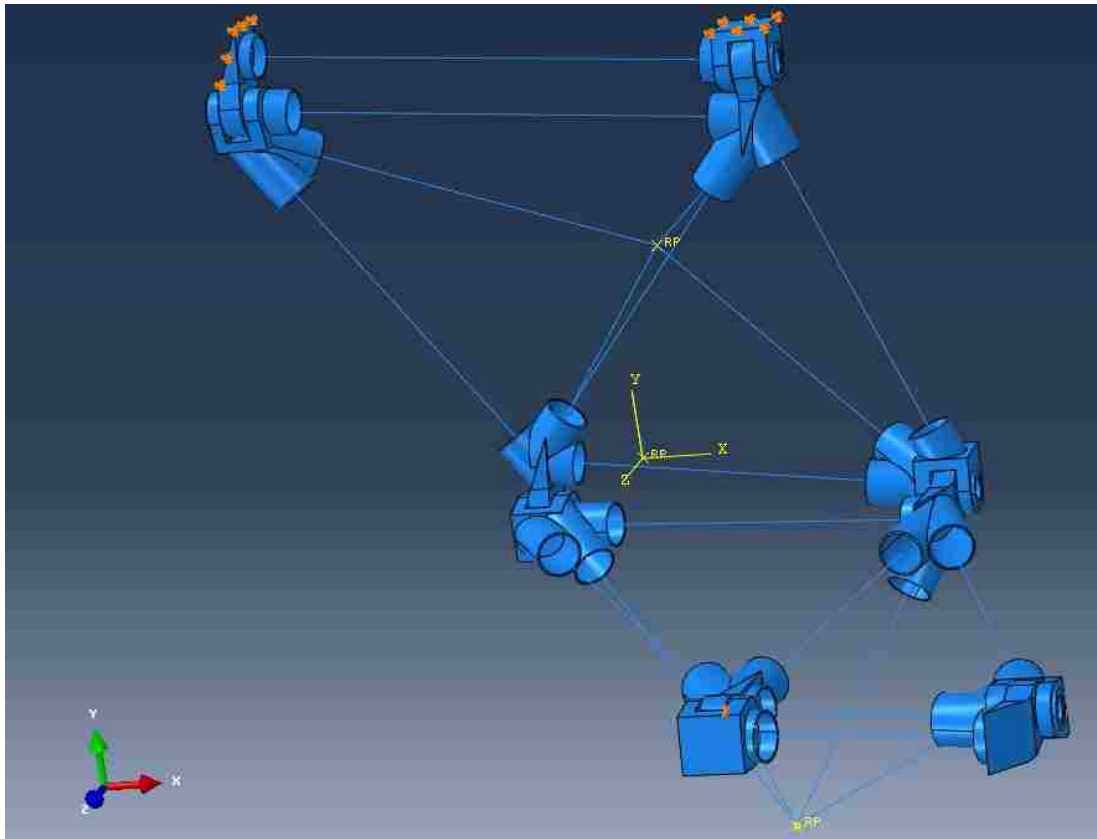


Fig.35 Simplified model

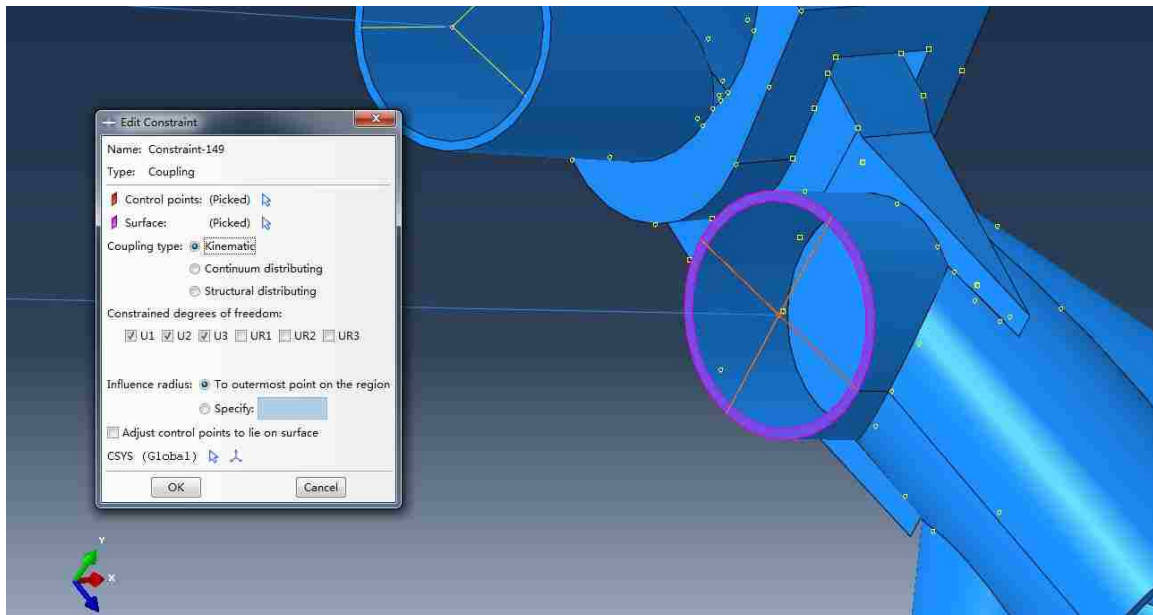


Fig.36 Diagram of coupling constraint

Since this analysis was slightly complex, many problems might happen in analysis process. Fig.37 shows stresses obtained from a tentative finite element analysis of this model. In this analysis, the load applied was -20,000N in X direction, which was considerably lower than the desired load -100,000N.

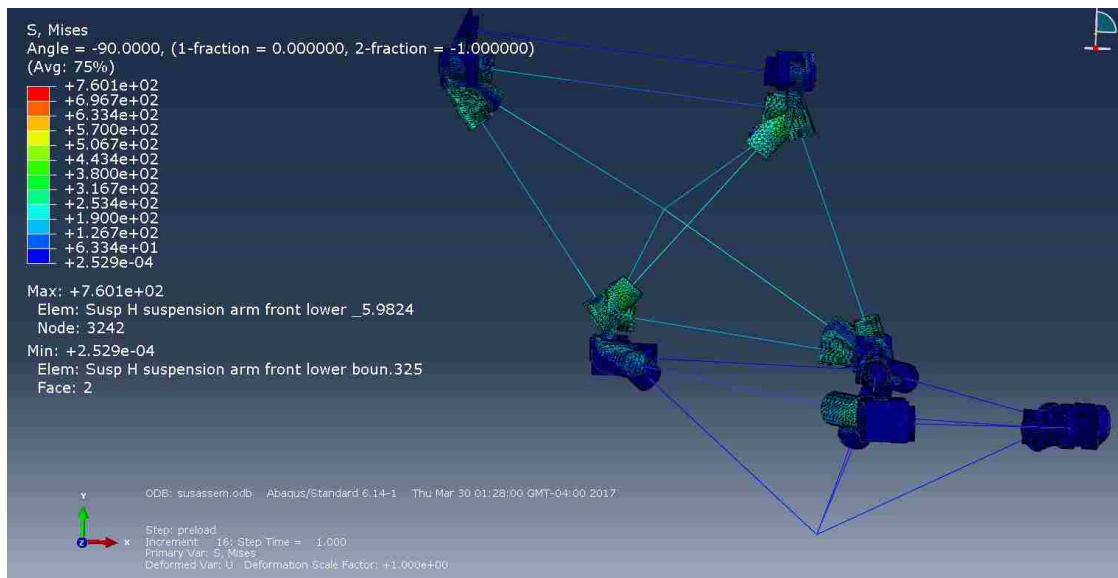


Fig.37 Tentative stress analysis result

## Simpler Model for Analysis

Despite the fact that total number of elements was reduced by 45% after the simplification, tentative simulation process still took more than 24 hours. Multiple contacts were involved in the simulation above. The accuracy of the simulation was not very good. In order to analyze the different load cases and study various wall thicknesses of the tubes etc, a simpler model that could be solved more quickly was desired.

---

A linear elastic truss (stick) model was made as shown in Fig.38. The element numbers of the two suspension arms are shown in Fig.38 and the node numbers in Fig.39. Boundary conditions and load were similar to them in the nonlinear analysis performed previously (Figs.32-33). In stick model, only two suspension links were model, with boundary conditions applied at some of its nodes of them. Node 1 is fixed, movements in Y and Z directions of node 2 and 8 were locked and load was applied on node 9. Forces on all elements under each load case were calculated and wall thicknesses of the tubes were adjusted to reduce mass or stress.

After analyzing the stick model, forces on all elements under different load cases were obtained. The load case under which the largest force occurred on tubes of the suspension links could be determined, and this load case is considered the worst operation condition of the boat. Then linear elastic analysis was performed to the whole suspension link model under this operation condition. By doing this, the validity of suspension links design under the worst operating condition could be verified.

### Analysis of Stick Model

In the stick model, tubes of the suspension links were represented by truss elements, which deform only in the axial direction (without any bending). The four joints in the suspension arms were neglected.

In the real boat suspension, it is not clear whether transverse loads are carried through joint A, joint B or both (it is statically indeterminate and depends on flange thickness and

---

stiffnesses of bushings, (weld) deformations of the links, etc). Therefore two different scenarios were studied: either all transverse load was carried by joint A, or by joint B. This means that either  $U_x^3 = U_x^6$  or  $U_x^4 = U_x^7$  in the analysis. All in all, eight different load cases were defined, and named 200a (the bottom of sponson hull is 200mm higher than the water surface at normal ride height and joint A takes all X-direction load ( $U_x^3 = U_x^6$ )); -100b (the bottom of sponson hull is 100mm lower than water surface at normal ride height and joint B takes all X-direction load ( $U_x^4 = U_x^7$ )), etc.

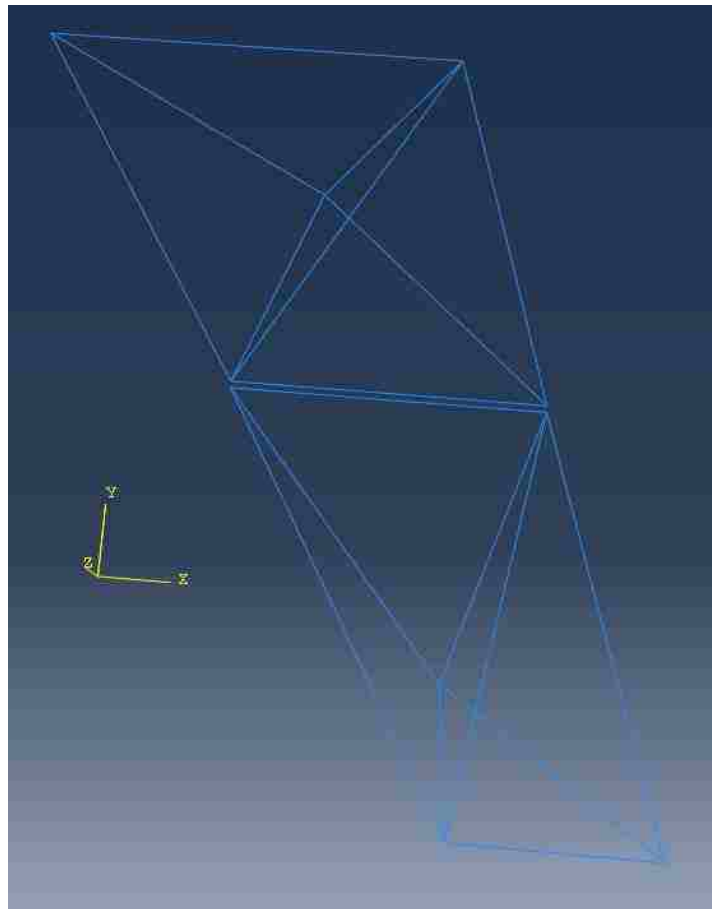


Fig.38 Stick model

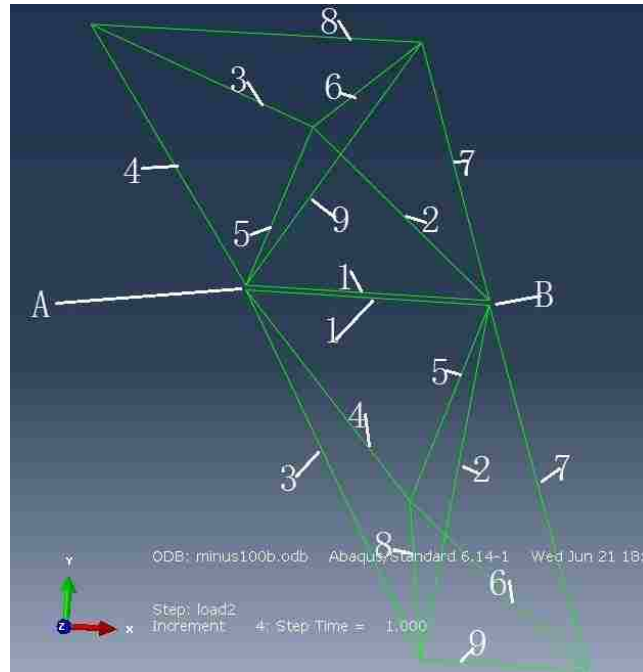


Fig.39 Element numbers for the upper and lower suspension links

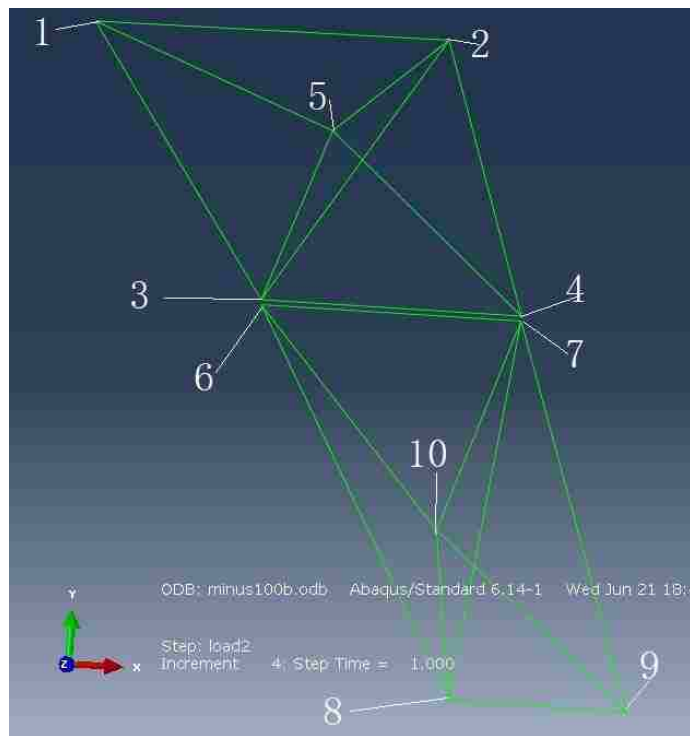


Fig.40 Node numbers

---

The boundary conditions are then:

At node 1:  $U_x = U_y = U_z = 0$

At node 2:  $U_y = U_z = 0$

At node 8:  $U_y = U_z = 0$

At node 9:  $F_x = -100,000N$

At node 3, 4, 6 and 7:  $U_y^3 = U_y^6$ ,  $U_z^3 = U_z^6$ ,  $U_y^4 = U_y^7$ ,  $U_z^4 = U_z^7$ , and  $U_x^3 = U_x^6$   
(if joint A takes load) or  $U_x^4 = U_x^7$  (if joint B takes load)

Performing linear elastic analysis of the stick model yielded the loads shown in Tables 4-11. In Abaqus, stresses at integration points of each element were obtained when analysis was done. Then variables like stress and force at node of the element were calculated.

In the stick model, forces on elements were displayed in the form of three components  $F_x$ ,  $F_y$ ,  $F_z$  at nodes of corresponding element. For example, force on element 1 of the upper arm could be measured at node 3 or node 4 (or anywhere in between). Since the elements were two-force members, the three components of force measured at node 3 were equal and opposite to corresponding components measured at node 4, in other words,  $F_x^3 = -F_x^4$ . All components of forces on elements were measured at the smaller-number node for convenience of arranging tables of forces on elements. For example, force on element 1 of upper arm was measured at node 3 (the opposite end is at node 4).

In the stick model, the initial analyses were performed with all tubes being 50.8x2.083 mm (2.0"x0.082"). The maximum axial force in a tube was then 401,000N. The corresponding normal stress would be higher than 1300MPa in the tube, which is

---

considerably higher than the ultimate stress of A316L stainless steel (560MPa). Wall thicknesses for all elements were then adjusted to ensure that the stress did not exceed the ultimate stress (or at least not by a considerable amount). This required a few iterations (changing wall thickness, re-running the FEA, evaluating stresses and changing wall thickness, etc). The final results are tabulated in Tables 4-11.

Table-4 Forces on elements for -100a load case

Element number (end nodes)	$F_x[N]$	$F_y[N]$	$F_z[N]$	$F[N]$	Wall thickness[mm]	Normal stress[MPa]
1 (34)	-151437	0	0	-151437	3.048	-331.188
2 (45)	-149638	131305	-48714	204952	3.048	448.226
3 (15)	121404	-39364	-106212	166040	3.048	363.126
4 (13)	-139666	222215	105497	-282870	3.048	-618.63
5 (35)	-40120	-131305	48714	-145683	2.413	-397.168
6 (25)	68354	39364	106212	-132298	2.032	-424.957
7 (24)	1798	-5182	-2640	6087	2.032	19.554
8 (12)	-81738	0	0	-81738	2.032	-262.552
9 (23)	-151891	-217033	-103037	284237	3.9624	487.504
1 (12)	-18349	0	0	-18349	2.032	-58.94
2 (23)	-18349	-136488	-46254	145275	2.032	466.643
3 (13)	-81620	136488	46254	-165621	2.032	-531.994
4 (15)	0	0	0	0	2.032	0
5 (25)	0	0	0	0	2.032	0
6 (45)	0	0	0	0	2.032	0
7 (24)	0	0	0	0	2.032	0
8 (35)	0	0	0	0	2.032	0
9 (34)	-100000	0	0	-100000	2.032	-321.211

Table-5 Forces on elements for -100b load case

Element number (end nodes)	$F_x[N]$	$F_y[N]$	$F_z[N]$	$F[N]$	Wall thickness[mm]	Normal stress[MPa]
1 (34)	-251437	0	0	-251437	3.048	-549.886
2 (45)	-149638	131305	-48714	204952	3.048	448.226
3 (15)	121404	-39364	-106212	-166040	3.048	-363.126
4 (13)	-139666	222215	105497	-282870	3.048	-618.63
5 (35)	-40120	-131305	48714	-145683	2.413	-397.168
6 (25)	68354	39364	106212	-132298	2.032	-424.957
7 (24)	1798	-5182	-2460	6011	2.032	19.31
8 (12)	-81738	0	0	-81738	2.032	-262.552
9 (23)	-151891	-217033	-103037	284237	3.9624	487.504
1 (12)	81650	0	0	81650	2.032	262.271
2 (23)	-18349	-136488	46254	145275	2.032	466.643
3 (13)	-81650	136488	-46254	-165635	2.032	-532.042
4 (15)	0	0	0	0	2.032	0
5 (25)	0	0	0	0	2.032	0
6 (45)	0	0	0	0	2.032	0
7 (24)	0	0	0	0	2.032	0
8 (35)	0	0	0	0	2.032	0
9 (34)	-100000	0	0	-100000	2.032	-321.211

Table-6 Forces on elements for 0a load case

Element number (end nodes)	$F_x[N]$	$F_y[N]$	$F_z[N]$	$F[N]$	Wall thickness[mm]	Normal stress[MPa]
1 (34)	-163264	0	0	-163264	3.048	-357.054
2 (45)	-170805	154142	-42377	233944	3.048	511.63
3 (15)	138577	-34233	-124681	189527	3.048	414.492
4 (13)	-139036	211256	123838	-281595	3.048	-615.841
5 (35)	-45795	-154142	42377	-166291	2.413	-453.35
6 (25)	78022	34233	124681	-151012	2.032	-485.07
7 (24)	-7541	20749	12163	-25206	2.032	-80.964
8 (12)	-99540	0	0	-99540	2.032	-319.735
9 (23)	-170022	-232005	-136001	318166	3.9624	545.697
1 (12)	-18349	0	0	-18349	2.032	-58.94
2 (23)	-18349	-133393	54541	145275	2.032	466.643
3 (13)	-81650	133393	-54541	-165635	2.032	-532.042
4 (15)	0	0	0	0	2.032	0
5 (25)	0	0	0	0	2.032	0
6 (45)	0	0	0	0	2.032	0
7 (24)	0	0	0	0	2.032	0
8 (35)	0	0	0	0	2.032	0
9 (34)	-100000	0	0	-100000	2.032	-321.211

Table-7 Forces on elements for 0b load case

Element number (end nodes)	$F_x[N]$	$F_y[N]$	$F_z[N]$	$F[N]$	Wall thickness[mm]	Normal stress[MPa]
1 (34)	-263264	0	0	-263264	3.048	-575.751
2 (45)	-170805	154142	-42377	233944	3.048	511.63
3 (15)	138577	-34233	-124681	189527	3.048	414.492
4 (13)	-139036	211256	123838	-281595	3.048	-615.841
5 (35)	-45795	-154142	42377	-166291	2.413	-453.35
6 (25)	78022	34233	124681	-151012	2.032	-485.07
7 (24)	-7541	20749	12163	-25206	2.032	-80.964
8 (12)	-99540	0	0	-99540	2.032	-319.735
9 (23)	-170022	-232005	-136001	318166	3.9624	545.697
1 (12)	81650	0	0	81650	2.032	262.271
2 (23)	-18359	-133393	54541	145277	2.032	466.647
3 (13)	-81650	133393	-54541	-165635	2.032	-532.042
4 (15)	0	0	0	0	2.032	0
5 (25)	0	0	0	0	2.032	0
6 (45)	0	0	0	0	2.032	0
7 (24)	0	0	0	0	2.032	0
8 (35)	0	0	0	0	2.032	0
9 (34)	-100000	0	0	-100000	2.032	-321.211

Table-8 Forces on elements for 200a load case

Element number (end nodes)	$F_x[N]$	$F_y[N]$	$F_z[N]$	$F[N]$	Wall thickness[mm]	Normal stress[MPa]
1 (34)	-173895	0	0	-173895	3.048	-380.303
2 (45)	-214329	199937	16265	293557	3.048	642.003
3 (15)	173889	13209	-161703	237822	3.048	520.112
4 (13)	-118207	132701	160419	-239409	3.048	-523.581
5 (35)	-57464	-199937	-16265	-208666	2.413	-568.874
6 (25)	97904	-13209	161703	-189493	2.032	-608.674
7 (24)	-40433	82198	99367	-135149	2.032	-434.114
8 (12)	-155682	0	0	-155682	2.032	-500.068
9 (23)	-213153	-214899	-259786	398879	3.9624	684.129
1 (12)	-18349	0	0	-18349	2.032	-58.94
2 (23)	-18349	-117739	83102	145276	2.032	466.643
3 (13)	-81650	117739	-83102	-165635	2.032	-532.042
4 (15)	0	0	0	0	2.032	0
5 (25)	0	0	0	0	2.032	0
6 (45)	0	0	0	0	2.032	0
7 (24)	0	0	0	0	2.032	0
8 (35)	0	0	0	0	2.032	0
9 (34)	-100000	0	0	-100000	2.032	-321.211

Table-9 Forces on elements for 200b load case

Element number (end nodes)	$F_x[N]$	$F_y[N]$	$F_z[N]$	$F[N]$	Wall thickness[mm]	Normal stress[MPa]
1 (34)	-273895	0	0	-273895	3.048	-599.001
2 (45)	-214329	199937	16265	293557	3.048	642.003
3 (15)	173889	13209	-161703	237822	3.048	520.112
4 (13)	-118207	132701	160419	-239409	3.048	-523.581
5 (35)	-57464	-199937	-16265	-208666	2.413	-568.874
6 (25)	97904	-13209	161703	-189493	2.032	-608.674
7 (24)	-40433	82198	99367	-135149	2.032	-434.114
8 (12)	-155682	0	0	-155682	2.032	-500.068
9 (23)	-213153	-214899	-259786	398879	3.9624	684.129
1 (12)	81650	0	0	81650	2.032	262.271
2 (23)	-18349	-117739	83102	145276	2.032	466.643
3 (13)	-81650	117739	-83102	-165635	2.032	-532.042
4 (15)	0	0	0	0	2.032	0
5 (25)	0	0	0	0	2.032	0
6 (45)	0	0	0	0	2.032	0
7 (24)	0	0	0	0	2.032	0
8 (35)	0	0	0	0	2.032	0
9 (34)	-100000	0	0	-100000	2.032	-321.211

Table-10 Forces on elements for 400a load case

Element number (end nodes)	$F_x[N]$	$F_y[N]$	$F_z[N]$	$F[N]$	Wall thickness[mm]	Normal stress[MPa]
1 (34)	-152467	0	0	-152467	3.048	-333.441
2 (45)	-207022	184486	59221	283549	3.048	620.115
3 (15)	167961	47947	-149195	229715	3.048	502.381
4 (13)	-93669	73487	147703	-189711	3.048	-414.893
5 (35)	-55505	-184486	-59221	-201551	2.413	-549.478
6 (25)	94566	-47947	149195	-183032	2.032	-587.923
7 (24)	-54554	77505	155780	-182347	2.032	-585.723
8 (12)	-174292	0	0	-174292	2.032	-559.846
9 (23)	-214304	-150993	-303483	401032	3.9624	687.822
1 (12)	-18349	0	0	-18349	2.032	-58.94
2 (23)	-18349	-106980	96558	145275	2.032	466.642
3 (13)	-81650	106980	-96558	-165635	2.032	-532.041
4 (15)	0	0	0	0	2.032	0
5 (25)	0	0	0	0	2.032	0
6 (45)	0	0	0	0	2.032	0
7 (24)	0	0	0	0	2.032	0
8 (35)	0	0	0	0	2.032	0
9 (34)	-100000	0	0	-100000	2.032	-321.211

Table-11 Forces on elements for 400b load case

Element number (end nodes)	$F_x[N]$	$F_y[N]$	$F_z[N]$	$F[N]$	Wall thickness[mm]	Normal stress[MPa]
1 (34)	-252467	0	0	-252467	3.048	-552.138
2 (45)	-207022	184486	59221	283549	3.048	620.115
3 (15)	167961	47947	-149195	229715	3.048	502.381
4 (13)	-93669	73487	147703	-189711	3.048	-414.893
5 (35)	-55505	-184486	-59221	-201551	2.413	-549.478
6 (25)	94566	-47947	149195	-183032	2.032	-587.923
7 (24)	-54554	77505	155780	-182347	2.032	-585.723
8 (12)	-174292	0	0	-174292	2.032	-559.846
9 (23)	-214304	-150993	-303483	401032	3.9624	687.822
1 (12)	81650	0	0	81650	2.032	262.271
2 (23)	-18349	-106980	96558	145275	2.032	466.642
3 (13)	-81650	106980	-96558	-165635	2.032	-532.041
4 (15)	0	0	0	0	2.032	0
5 (25)	0	0	0	0	2.032	0
6 (45)	0	0	0	0	2.032	0
7 (24)	0	0	0	0	2.032	0
8 (35)	0	0	0	0	2.032	0
9 (34)	-100000	0	0	-100000	2.032	-321.211

---

## Linear Analysis of Suspension Links

The stick model described above was used to determine wall thickness of tubes, as well as the worst load case. The worst load case of those analyzed (see section “Analysis of Stick Model”) was when the sponson was deflected 400mm.

A new FE model was developed. It was essentially identical to the one shown in Fig.35, but a linear elastic analysis was performed. Rather than using contact conditions between pins, bearings etc, they were “bonded” (rigidly connected) or sliding. In particular, three cases were analyzed:

- I. All bearings and pins were bonded at joint A (the inboard joint as shown in Fig.41). At joint B, sliding in the X direction was allowed. This was done in the FE model by forcing the average deflection of the bearing surfaces of the two parts of the joint to be equal, both in Y and Z directions. The case analyzed is called 400ax (similar to case 400a in the stick model).
- II. Joint A sliding and joint B bonded, called case 400bx.
- III. Both joint A and B were bonded, called 400abx.

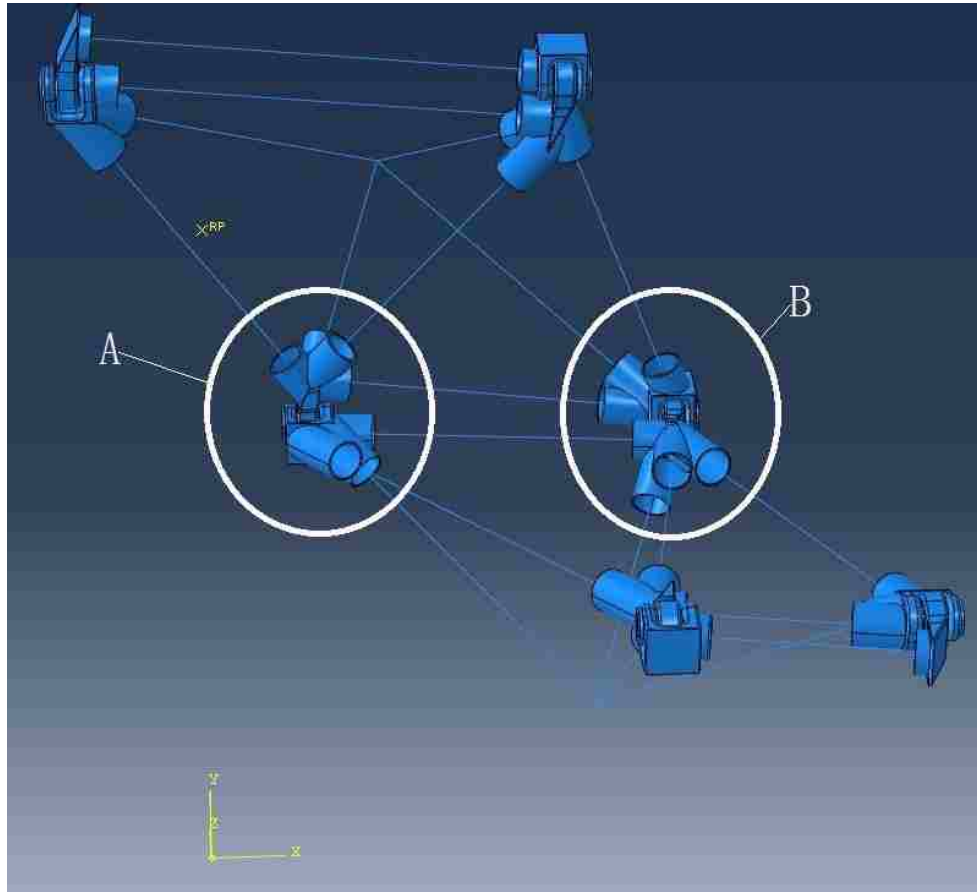


Fig.41 The latest FE model. Joints A and B are circled

Analysis results under load case 400ax is shown in Fig.42. The stress by joint A of this analysis is shown in Fig.43. By comparison, the stress at joint B under load case 400bx is shown in Fig.44, and stresses by both joint A and B under load case 400abx are shown in Figs.45-47. These were the worst cases.

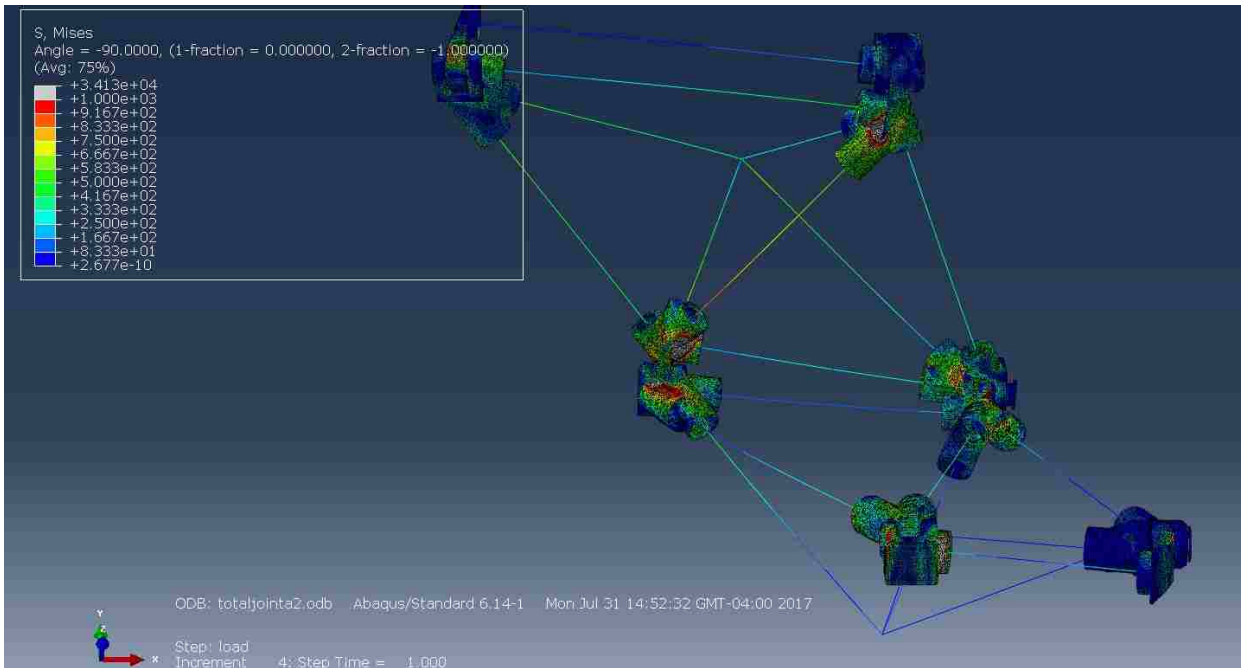


Fig.42 Analysis results under load case 400ax

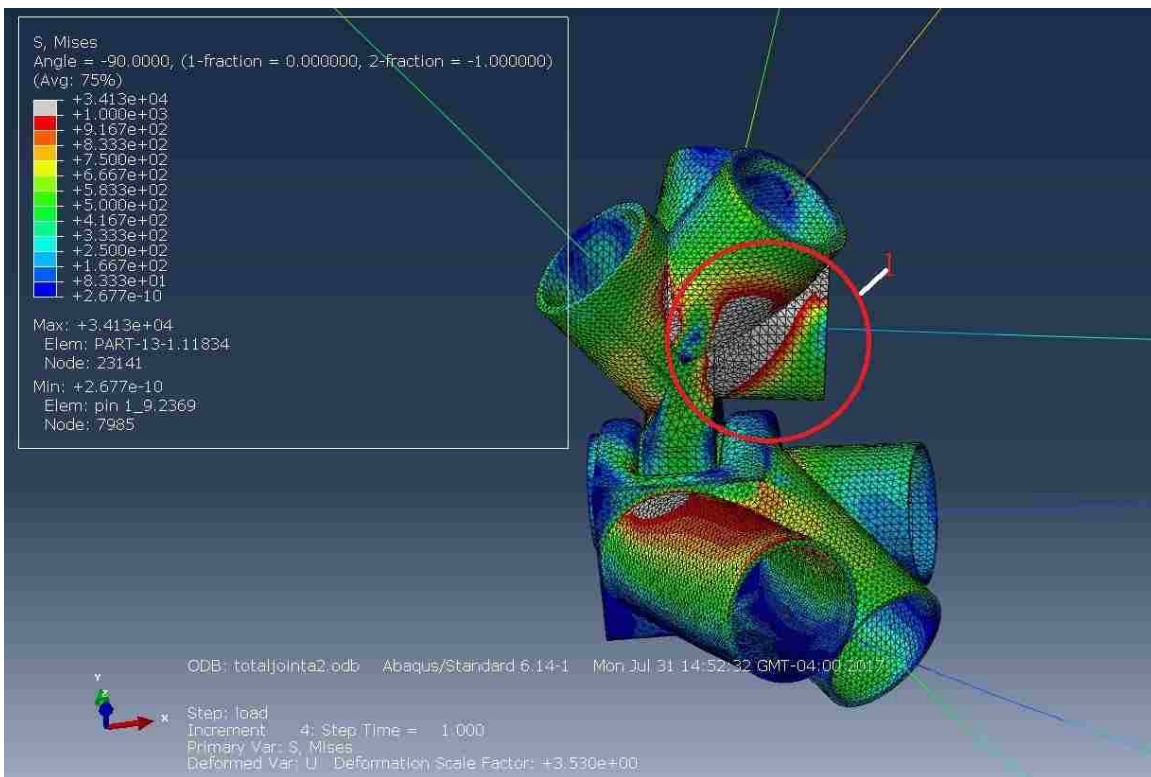


Fig.43 Stresses by joint A for 400ax

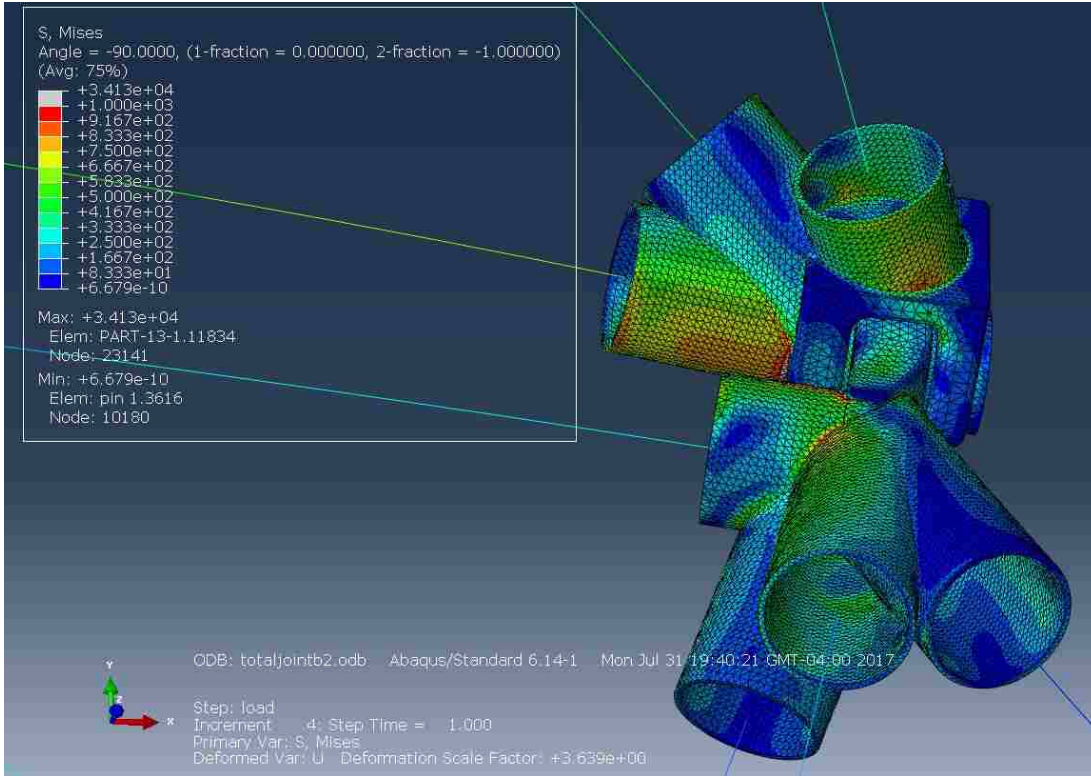


Fig.44 Stresses by joint B for 400bx

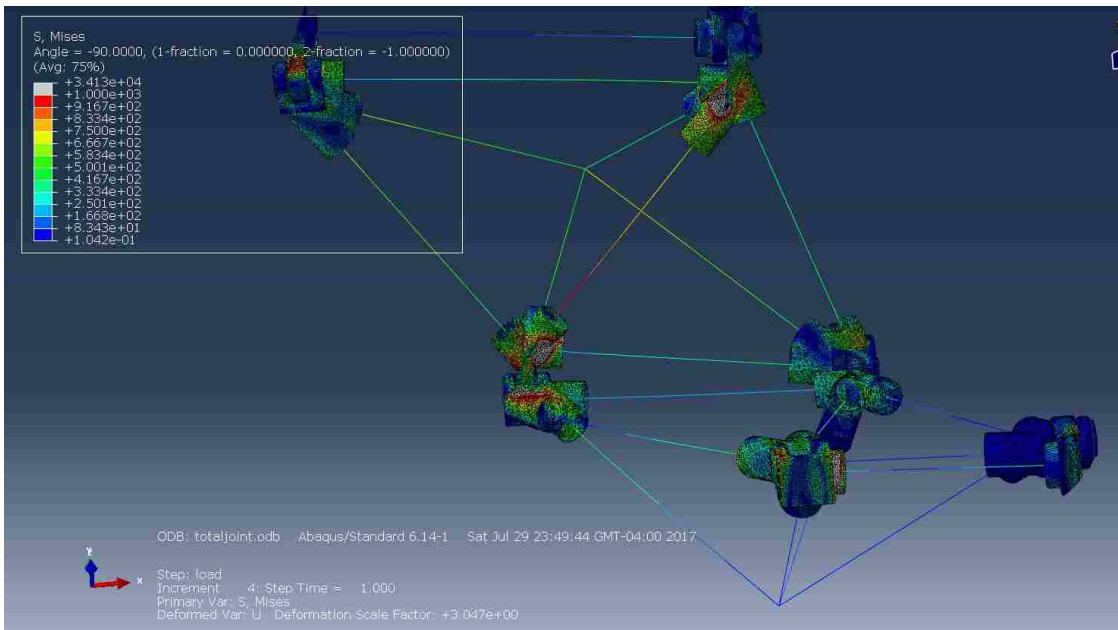


Fig.45 Analysis Results of Joint A and B for case 400abx

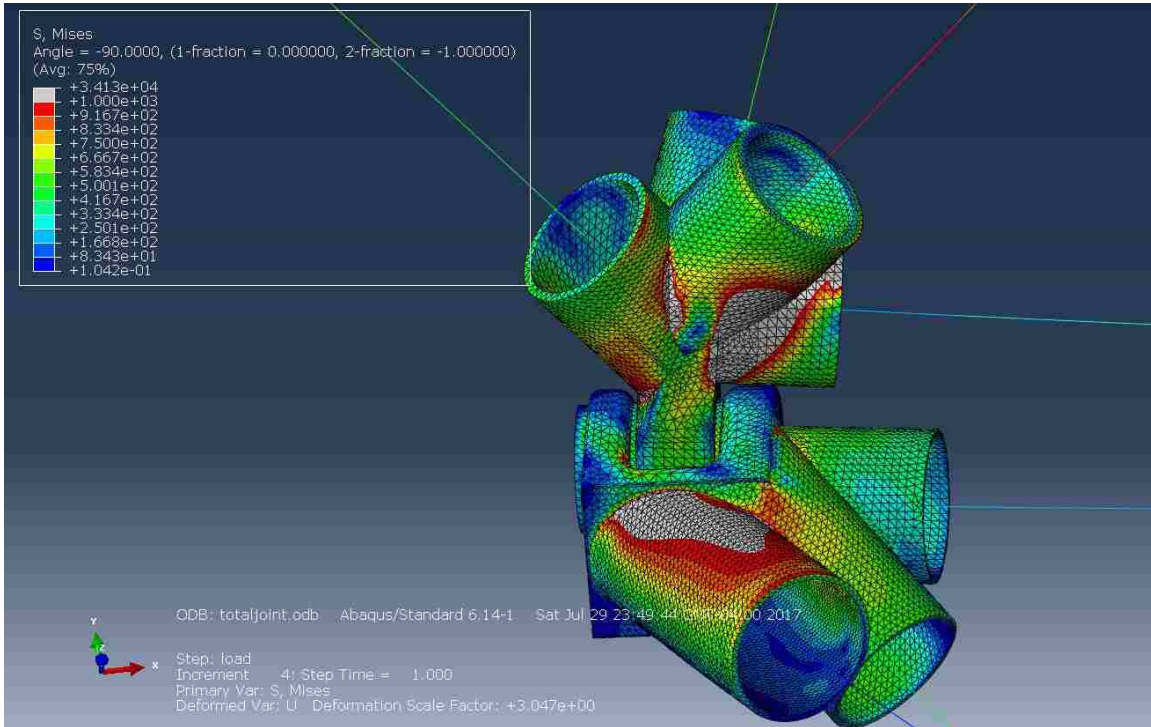


Fig.46 Stresses by joint A for 400abx

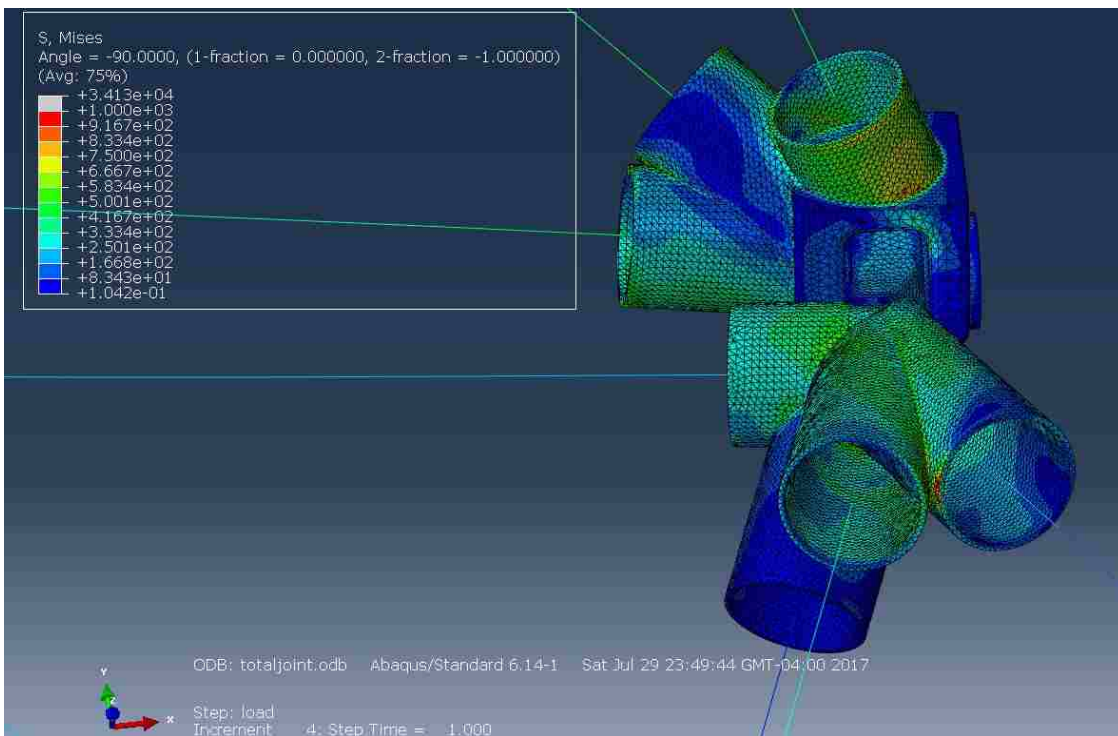


Fig.47 Stresses by joint B for 400abx

---

## Results Analysis of Linear Elastic Simulation

- I. High stresses were found at joint A as shown in Fig.48. Within the white circle the maximum stress reached approximately 1000MPa. However, stresses in the remainder of this part were lower than the ultimate stress of the material as shown in Figs. 48-49. Further, high stresses were found at edge of tubes (for example within the black circle). Increasing wall thickness of this tube at this place is expected to decrease the stresses there.

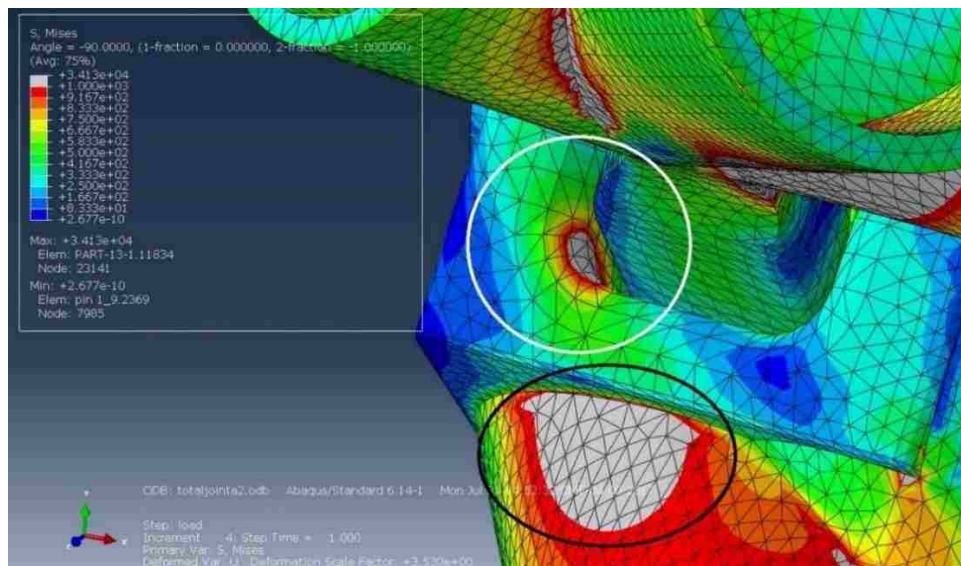


Fig.48 Stress concentrations by joint A

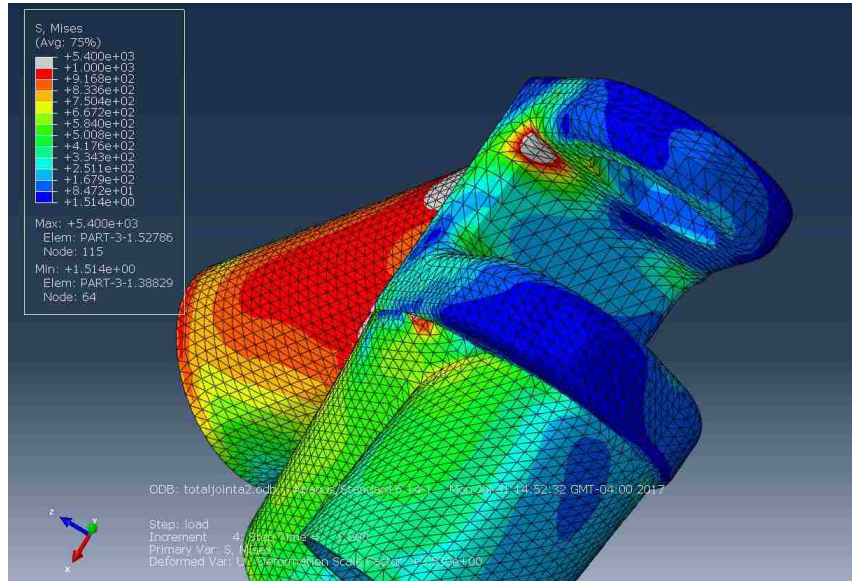


Fig.49 Stresses in joint A

- II. Comparing stress distribution in Fig.43 and Fig.44, the stress is higher in joint A under load case 400ax than in joint B under load case 400 bx. This indicates that it may be beneficial to design the suspension links such that joint B carries most of the transverse load rather than joint A.
  
- III. Comparing Fig.46 and Fig.47, it is seen joint A was more highly stressed than joint B when both joints were bonded (load case 400abx). This further indicates that it may be beneficial if joint B carries most of the transverse load.

---

## Conclusion

- I. A bung used to bolt suspension components to the center hull of a suspension boat were analyzed and re-designed. A set of parameters suitable for all load cases was determined. All bungs have been manufactured.
- II. Several methods were used to analyze the suspension links but most of them were not very successful. In the end a scheme was devised to analyze the suspension links using linear analyses. It is believed that this approach is sufficient for design of the suspension components.
- III. Wall thickness of tubes of suspension links was adjusted to reduce excessive stress happened on them.
- IV. Based on linear analysis results, the joints appear to be of sufficient strength if some plastic deformation is allowed under the most extreme loads. Extreme loads are not expected to occur often so some local plastic deformation can be tolerated.

---

## References

- 1.1 Grenestedt J.L., “Suspension Boat Dynamics”, Trans RINA, Vol 155, Part B1, Intl J Small Craft, Jan-Jun 2013.
- 1.2 Grenestedt J.L., “Boat Suspension” US Patent 20100000454.